Analyzing the Impact of Streamflow Drought on Hydroelectricity Production: A Global-Scale Study

Wenhua Wan[1,2], Jianshi Zhao[1], Eklavyya Popat[3], Claudia Herbert[3], and Petra Döll[3,4]

[1]Department of Hydraulic Engineering, State Key Laboratory of Hydro-Science and Engineering, Tsinghua University, Beijing, China, [2]School of Environment and Civil Engineering, Dongguan University of Technology, Guangdong, China, [3]Institute of Physical Geography, Goethe University Frankfurt, Frankfurt am Main, Germany, [4]Senckenberg Leibniz Biodiversity and Climate Research Centre Frankfurt (SBiK-F), Frankfurt am Main, Germany

Abstract Electricity production by hydropower is negatively affected by drought. To understand and quantify risks of less than normal streamflow for hydroelectricity production (HP) at the global scale, we developed an HP model that simulates time series of monthly HP worldwide and thus enables analyzing the impact of drought on HP. The HP model is based on a new global hydropower database (GHD), containing 8,716 geo-localized plant records, and on monthly streamflow values computed by the global hydrological model WaterGAP with a spatial resolution of 0.5°. The GHD includes 44 attributes and covers 91.8% of the globally installed capacity. The HP model can reproduce HP trends, seasonality, and interannual variability that was caused by both (de)commissioning of hydropower plants and hydrological variability. It can also simulate streamflow drought and its impact on HP reasonably well. Global risk maps of HP reduction were generated for both 0.5° grid cells and countries, revealing that 67 out of the 134 countries with hydropower suffer, in 1 out of 10 years, from a reduction of more than 20% of mean annual HP and 18 countries from a reduction of more than 40%. The developed HP model enables advanced assessments of drought impacts on hydroelectricity at national to international levels.

1. Introduction

Electricity production by hydropower plants harnesses the energy of flowing water, a renewable source for electricity production. In case of most hydropower plants, greenhouse gas emissions per kWh of generated electricity, mainly caused by methane emissions from reservoirs behind hydropower dams, are much smaller than emissions caused by fossil fuel-based electricity production (IHA, 2018). Hydroelectricity production (HP) continuously increased from 1,296 TWh in 1973 to 4,170 TWh in 2016 (IEA, 2019). In 2016, HP accounted for 16.3% of the worldwide gross electricity production and for 67.1% of all renewable electricity production, while it is expected to increase by 2.5%/year through 2030 (IEA, 2019). In 2017, installed hydropower capacity increased by 1.7% compared to the year before; almost half of the growth came from China. Even though ecological impacts of hydropower stations can be considerable (e.g., Benejam et al., 2016; Bunn & Arthington, 2002), expansion of hydropower may be suitable for providing electricity in a low-carbon society, in particular in least developed and electricity-poor countries (UNCTAD, 2017).

Unfortunately, there is no comprehensive data sets of hydropower plants open to public which comprises information on location, capacity, maximum hydraulic head, and other basic characteristics of hydropower plants on a global scale. Van Vliet, Wiberg, et al. (2016), Van Vliet, van Beek, et al. (2016), and Van Vliet, Sheffield, et al. (2016) performed studies on global HP based on a database (UDI, 2013) that is not free of charge and only covers 78% of the total global hydropower installed capacity.

In hydropower plants, the potential energy of the water flowing through turbines with a certain vertical fall (termed hydraulic head) is converted into electricity. HP is a function of the product of hydraulic head and water flow but constrained by the technical installed capacity. Most HP is generated by impounding water behind dams (or weirs), which enables control of water driving the turbines and leads to an increased hydraulic head. Run-of-river hydropower plants rely on uncontrolled streamflow and generally, but not always, have a lower hydraulic head (some run-of-river plants have dams and canals leading to a hydraulic head of over 200 m). So-called pumped-storage hydropower plants utilize electrical energy produced by low-cost off-peak electricity to pump water to a reservoir at a higher elevation and release later at peak times.

Writing – review & editing: Wenhua Wan, Jianshi Zhao, Petra Döll

Both hydraulic head and water flows are temporally variable. In case of run-of-river hydropower, lower than normal streamflow, that is, drought, immediately reduces outflow through turbines and thus HP, while in case of reservoir-storage hydropower, lower than normal streamflow flowing into the reservoir may require a reduction of reservoir outflow and thus HP only later. Still, unless streamflow deficit is small compared to the reservoir storage, HP is reduced during streamflow drought for both types of hydropower plants, negatively affecting both hydropower suppliers and consumers. The three consecutive years of drought that began in 2014 had caused severe reductions in hydroelectricity supply with negative effects on daily life and the economy in Venezuela (Hambling, 2016). Two consecutive monsoon failures had reduced reservoir storage in India such that HP was significantly lower than normal in 2015–2016, with 15% less HP than the previous year in some plants, while electricity demand due to a heat wave (often concurrent to less precipitation than normal) was higher than normal (Singh & Sally, 2020). HP reduction due to drought is particularly problematic in countries that strongly rely on hydropower for their electricity supply, which include many countries in Africa and South America (EIA, 2019). For the western United States, it was found that frequent droughts had caused a notable shift toward conventional energy sources, thus leading to increases in air pollutant emissions of around 10% (Herrera-Estrada et al., 2018).

There are a number of continental- or global-scale studies about the impact of climate change on the potential of HP (e.g., Stanton et al., 2016; Van Vliet, van Beek, et al., 2016; Van Vliet, Wiberg, et al., 2016). Impact of drought on HP was only investigated for small regions and some countries such as Finland (Jääskeläinen et al., 2018) and Canada (Bonsal et al., 2011) and in one global study of Van Vliet, Sheffield, et al. (2016), HP reduction in selected drought years was quantified.

This paper presents a new comprehensive global hydropower database (GHD) and a global HP model to assess the impact of drought on HP. Combining data from the GHD and hydrological variables simulated by the global hydrological model WaterGAP (Müller Schmied et al., 2021), the HP model computes, with a spatial resolution of 0.5° (55 km × 55 km at the equator), monthly time series of HP between 1975 and 2016 at the global scale. The aim of this paper is to show and discuss the capability of the HP model and to assess HP reduction due to drought, computing HP reduction during spatially extensive historic drought events as well as the HP reduction that can be expected with a probability of 10% in 0.5° grid cells and whole countries. Section 2 describes the methodology consisting of the GHD and HP model development as well as drought and risk analyses. Section 3 validates the performance of the database and HP model, followed by the assessment of HP reduction due to drought. Section 4 discusses the uncertainties of the HP model and the robustness of the results. Section 5 closes with concluding remarks.

2. Methods and Data

The amount of hydropower electricity HP_t (kWh) produced over a time period H_t can be quantified using the following equation (El-Hawary & Christensen, 1979; Wan et al., 2020; Zhao et al., 2014):

$$HP_t = \min\left(\eta Q_{t,turb} H_t, N_{installed}\right) \cdot \Delta t \tag{1}$$

where η is a comprehensive hydropower coefficient (kJ m^{-4} = kN m^{-3}) that combines acceleration of the earth (m s^{-2}), density of water (kg m^{-3}) and a unitless efficiency term, $Q_{t,turb}$ is rate of water flow through the pipe and turbine (m^3/s), H_t is hydraulic head with respect to the outlets of the pipe (m), that is, the difference between elevations of forebay and tailwater, and $N_{installed}$ is the installed capacity of the hydropower plant (kW = kJ s^{-1}), that is, the maximum power output that can be produced by a specific plant. To enable the application of Equation 1 for simulating HP globally from 1975 onward, the location, type, and installed capacity of ideally all but at least a large part of all hydropower plants are required. H_t and $Q_{t,turb}$ must be estimated for all hydropower plants and time steps. As daily values of streamflow that are simulated by global-scale hydrological model are much less reliable than monthly values, HP is simulated with a monthly time step based on monthly streamflow simulated by the global hydrological model WaterGAP. The spatial resolution of the HP model is the spatial resolution of WaterGAP, 0.5° longitude × 0.5° latitude. WaterGAP streamflow values can be assumed to represent $Q_{t,turb}$ of the hydropower station within the grid cell as WaterGAP also simulates the water balance of large reservoirs. H_t of all considered hydropower

plants is derived from databases, topographic data, and WaterGAP simulation of water storage in reservoirs. Thus, HP model presented and applied in this study relies on two main inputs, the newly developed GHD (Section 2.1) and output of WaterGAP (Section 2.2). The HP model is introduced in Section 2.3.

2.1. A New Global Hydropower Database

Despite the recognition of environmentally sustainable hydropower to modern society, there is no reliable, comprehensive, and open-access global database describing hydropower plants and their characteristics. To address this shortcoming, we collated information about currently developed/under-construction hydropower plants in the new GHD.
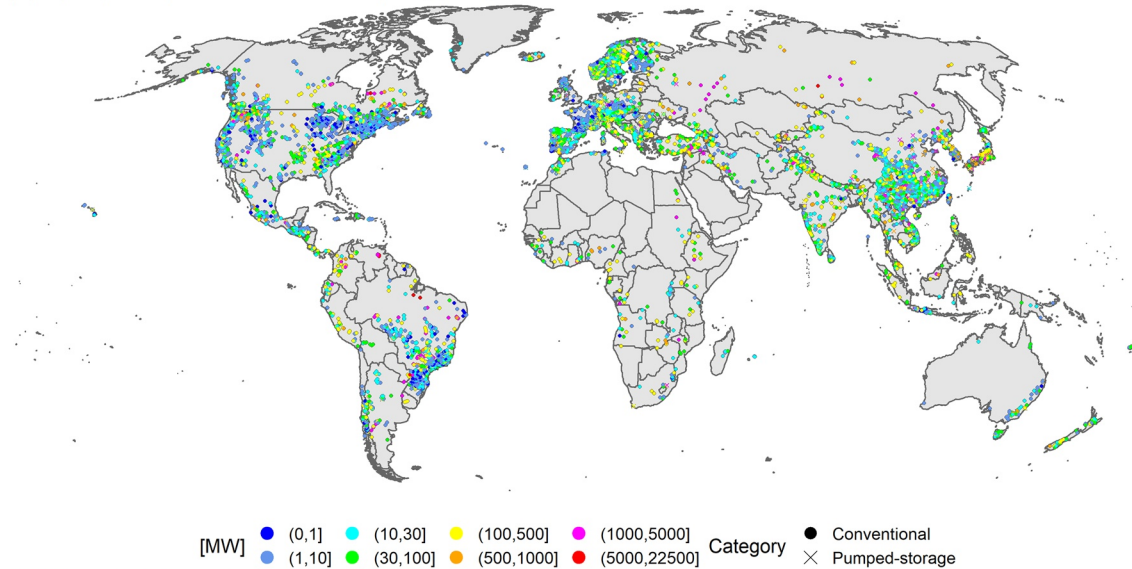
The GHD contains 8,716 records of hydropower plants distributed across 134 countries worldwide, consisting of 13.1% reservoir-storage plants, 9.9% run-of-river plants, and 3.3% pumped-storage plants. For the remaining 73.7% of plant records, no plant category is available, but we can assume that they are conventional plants (reservoir storage or run-of-river) as the installed capacity of pumped-storage plants fits EIA statistics well. A hydropower plant may be described by more than one record if it is located at the boundary of two countries or its installed capacity varied over time (Section S1). The total number of hydropower plants included in GHD is 8,648. The GHD comprises only hydropower plants with installed capacities above 1 MW or plants of which the associated reservoir has a storage capacity above 0.1 km^3. The spatial distribution and installed capacities of the hydropower plants included in GHD are shown in Figure 1a. The total installed capacity of all hydropower plants commissioned before 2016 is 1.147 TW, contributing 91.8% of the documented data of EIA (2019). 36.5% of total installed capacity is known to be reservoir-storage hydropower, 10.7% is run-of-river hydropower, and 13.4% is pumped-storage hydropower. For 39.4% of total installed capacity, the primary sources do not provide information on the category of hydropower plant. In some countries, HP accounts for more than 90% of total electricity production in 2016, while only a few countries do not harness hydropower at all (Figure 1b).

The GHD leverages a wide variety of sources. Most information was taken and merged from freely available databases including World Power Plants Database (WPPD) (Global Energy Observatory, 2019), Global Power Plant Database (GPPD) (World Resources Institute, 2018), and Global Reservoir and Dam Database (GRanD) version 2019 (Lehner et al., 2011) (compare Table S1). We also included plants that are not listed in these databases from scattered data sources, such as HTML sources (e.g., Wikipedia), NHA (https://www. hydro.org/map/hydro/), AQUASTAT (http://www.fao.org/aquastat/), CDM (https://cdm.unfccc.int/), or research articles (see Section S1 for more details). In addition to the compilation of data from these sources, GHD also contains estimated values as not all data required to implement Equation 1 were available from the data sources. The GHD contains 44 attributes per hydropower plant. Table 1 provides an overview of key attributes provided in the GHD, while a complete attribute list is found in Table S2.

Each hydropower plant and, if any, the associated reservoir was allocated to the appropriate 0.5° × 0.5° grid cell. This cannot be done by just taking into account latitude and longitude information of the plants but each plant has to be coregistered in accordance with the river network used in WaterGAP, the 0.5° global drainage direction map DDM30 (Döll & Lehner, 2002). Coregistration means that a power plant is assigned to a 0.5° grid cell not simply according to the geographic coordinates but taking into account its location on the actual river network (e.g., whether is located on the mainstem or the tributary entering the mainstem within the grid cell). Coregistration may move the plant to an adjacent cell to make sure that the plant is situated along the correct DDM30 river. It required extensive manual checking. For plants with information on the upstream basin, additional adjustments to the plant geographical location were implemented to ensure reasonable consistency: (1) the upstream catchment area defined by the DDM30 and those collected (partly) in GHD should be consistent or close; (2) compare the reservoir-storage capacities of plants in GHD to GRanD reservoirs, that is, the plants should be located in the outflow cells of GRanD reservoirs. Therefore, geo-locations and upstream and downstream topologies of some plants may be modified a bit as compared to their original sources.

For computing HP according to Equation 1, GHD included WaterGAP-derived attributes like catchment area, routing area, basin ID, the simulated long-term mean highest and lowest monthly streamflow at all 8,716 plant sites, and the simulated mean reservoir storage for 693 plant sites. Also included in GHD is the

(a) Hydropower plant and installed capacity [MW]

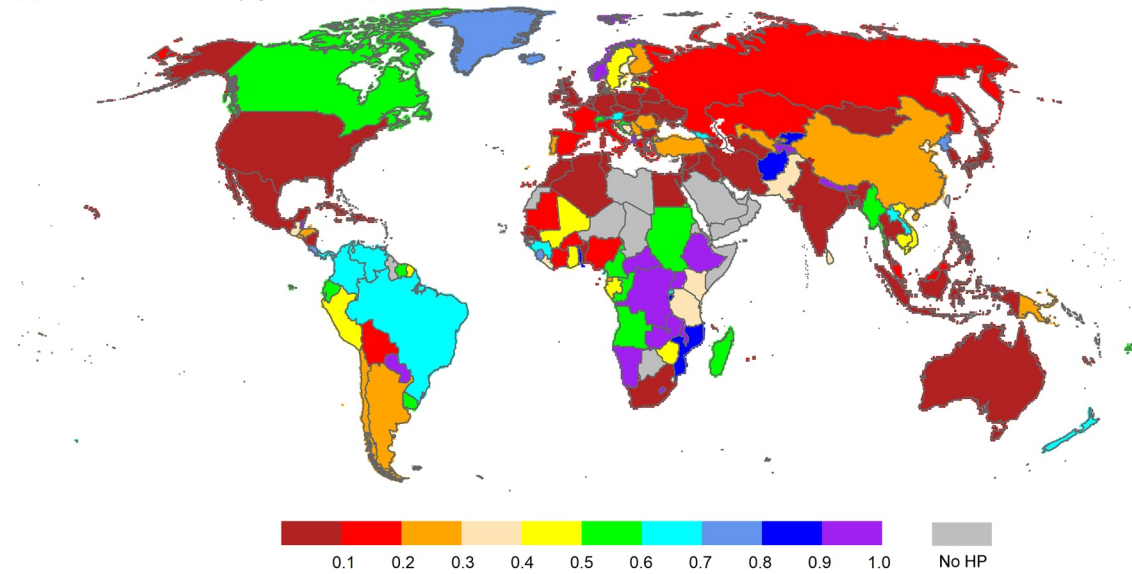
(b) HP to total electricity generation (2016)

Figure 1. Installed capacity and plant category of the hydropower plants included in GHD (a), and the conventional HP as a fraction of total electricity generation $r(HP)$ in countries in 2016 according to International Energy Statistics (EIA, 2019) (b). Conventional plants include both reservoir-storage and run-of-river plants. GHD, global hydropower database; HP, hydroelectricity production.

gridded elevation difference (H_{ele}, in meters) between the cell where the hydropower plant is located and the downstream cell, as this parameter was needed to estimate H_t (Equation 1 and Section 2.3) for many hydropower plants. The H_{ele} was computed based on HydroSHEDS, a 30-arc-second global digital elevation map (Lehner et al., 2006) distinguishing cells with flow direction to its downstream neighbor (i.e., cross-flow cells) from those cells without downstream cell (i.e., outflow cell of basin to the ocean or its inland sink). The elevation difference of the cross-flow cell was calculated by assuming streamflow falls from the mean elevation of the considered cell to that of the downstream neighboring cell (i.e., $H_{ele} = \Delta L_{mean}$, where L is the grid cell elevation in meters). In contrast, the streamflow for the basin-outflow cell is assumed, on average, falls from the mean elevation to the minimum elevation per cell; the elevation difference was then derived as the difference between the two elevations of the basin-outflow cell (i.e., $H_{ele} = L_{mean} - L_{min}$). Additionally, for 36 of the 60 largest hydropower plants with an installed capacity of at least 3,000 MW, the hydropower load factor (%) could be included in GHD (Table 1). The load factor, also known as capacity

Table 1
Overview of the Content of GHD, Providing the Number of Hydropower Plants for Which Key Attributes Are Available, the Percentage of Global Installed Capacity Covered, and the Sources of the Data

Key attributes/description	No. of plant record	$N_{installed}$ covered (%)	Sources
Plant name, geo-location, nominal, and actual installed capacities	8,716	100	Various sources, regression model for 500 stations
Maximum hydraulic head (H_{max})	971	31	Wikipedia, CDM
Dam/weir height (H_{dam})	4,169	76.6	GRanD, others
Commissioning year (first year plant generated electricity)	5,486	90.5	GPPD, others
Dividing opening years with specific operational status (short operation, recommission, damaged, refurbish, and unfinished)	93	8.1	Others
Started operation after 2016	42	4.5	Others
With information on plant category (reservoir storage, run-of-river, and pumped storage)	2,292	60.8	WPPD, Wikipedia
Annual HP estimation	7,012	86.2	GPPD, Wikipedia
Load factor	36	5.2	Cazzaniga et al. (2019), Wikipedia
Reservoir-storage capacities, surface area, mean streamflow, and upstream catchment area	2,347	53.3	GRanD, others
Reservoir operation is explicitly simulated in WaterGAP	716	29.4	GRanD, WaterGAP

Note. Details on data sources are provided in Section S1 and Table S1. A complete list of attributes is provided in Table S2.

factor or percentage full load hours, is calculated as actual annual HP divided by the theoretical maximum annual HP. The load factor of the 36 plants varies between 36% and 80%. Taking into account the load factor enabled a good reproduction of recorded HP for these large plants.

2.2. WaterGAP

WaterGAP 2.2d (Müller Schmied et al., 2021) is a 0.5° (55 km × 55 km at the equator) grid-based global-scale hydrological model that simulates both human water use and freshwater fluxes and water storages on all continents of the Earth except Antarctica with a daily time step. Differentiating surface water bodies and groundwater as sources and sinks of water withdrawals, it estimates water withdrawal and consumption for five sectors: irrigation, livestock farming, domestic use, manufacturing water use, and thermal power plant cooling (Döll et al., 2014). Based on the simulated time series of net groundwater, time series of climate data and many physiographical data, daily water balances of up to 10 storage compartments are computed for each of the 67,420 grid cells. For this study, the global daily WFDEI-GPCC data set (Weedon et al., 2014) was used as climate input. Runoff from land is routed through groundwater and surface water bodies (i.e., lakes, reservoirs, wetlands, and rivers) along the drainage direction. WaterGAP simulates water storage dynamics of and outflow from the 1,109 largest reservoirs worldwide (storage capacity ≥0.5 km³) and 52 regulated lakes (area ≥100 km²) based on the GRanD database version 1.1 (Lehner et al., 2011; Müller Schmied et al., 2021). Seven hundred and five of the 1,161 large reservoirs/regulated lakes have HP as either the most important or the second most important purpose. Simulation of reservoir operation in WaterGAP distinguishes reservoirs with the main purpose of irrigation from all others (Döll et al., 2009). WaterGAP 2.2d also includes more than 5,000 man-made reservoirs, whose storage capacities are less than 0.5 km³. In each grid cell, the water balance of these small reservoirs and of all small lakes is simulated by a lake algorithm (Müller Schmied et al., 2021). Different from other global hydrological models, WaterGAP is calibrated against observed long-term average annual streamflow at 1,309 gauging stations, with the purpose of obtaining meaningful estimates of water resources despite a number of sources for significant uncertainty in global hydrological modeling (Müller Schmied et al., 2014). This is one of the reasons why WaterGAP has been shown to provide better fits to streamflow observations than most other global hydrological models (Krysanova et al., 2020; Zaherpour et al., 2018).
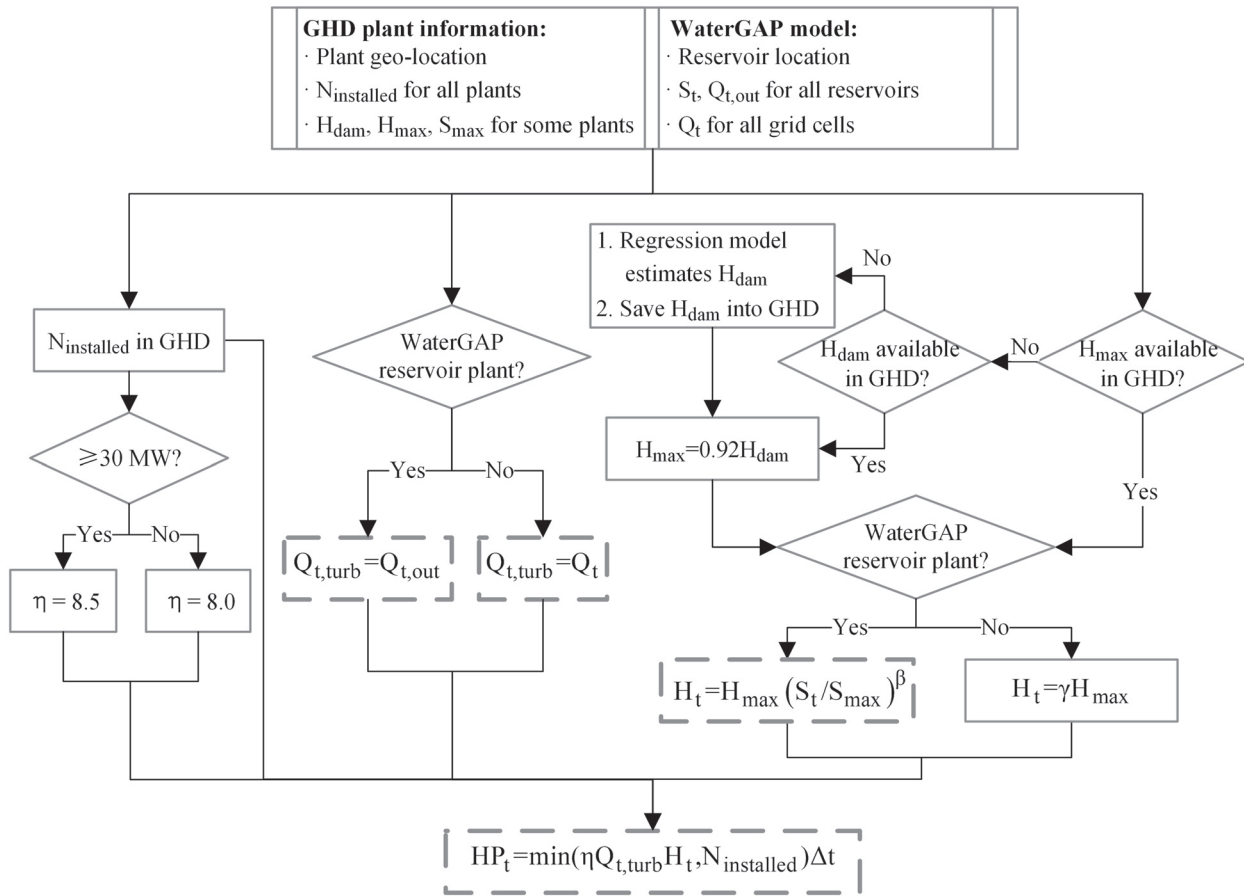
Figure 2. HP simulation process using GHD and WaterGAP data as input. Boxes with solid lines indicate temporally constant variables, and those with dashed lines indicate monthly time series. HP, hydroelectricity production; GHD, global hydropower database.

WaterGAP output used for the HP model includes time series of streamflow Q_t (impacted by human water use and man-made reservoirs) for each grid cell as well as time series of outflow $Q_{t,out}$ and water storage S_t of the 705 large reservoirs with the purpose of HP (relating to 22 pumped-storage and 694 conventional power plants in GHD, one conventional plant only commissioned after 2016) for the period 1975–2016. Monthly time series aggregated from daily values served as input for the HP model.

2.3. HP Model

The developed HP model takes into account only conventional hydropower plants, that is, reservoir-storage and run-of-river plants. The electricity produced by the pumped-storage plants is not included in this study because (1) pumped-storage plants do not produce net electricity but serve as energy storages (House et al., 2018), and (2) data for calculating pumped-storage HP such as operating period, pumping rate as well as lift and drop heights (Schill & Kemfert, 2011) are lacking.

Based on Equation 1, the HP model simulates monthly time series of HP for each conventional hydropower plant in GHD. It does not distinguish run-of-river plants from reservoir-storage plants as there is no information on plant category for 73.7% of the plants in GHD, corresponding to 39.4% of total installed capacity. Figure 2 provides the flowchart of plant-specific HP simulation. To implement Equation 1, the comprehensive hydropower coefficient η, which usually ranges from 6.5 to 8.5 kJ m^{-4} depending on water conduit and turbine types (Bakis, 2007; Zhou et al., 1997), is set to 8.5 kJ m^{-4} for large hydropower plants with an installed capacity $N_{installed}$ of more than 30 MW (Department of Energy, 2019) and to 8.0 kJ m^{-4} for smaller plants. The time step interval is set to 1 month assuming nonstop HP (i.e., Δt =1 month). For the 36 large

plants with known load factor, we reduced the time interval by multiplying it with the load factor. Turbine release $Q_{t,turb}$ is specified for two cases. For the 693 WaterGAP reservoir plants whose reservoir operation processes are explicitly simulated in WaterGAP 2.2d, we assume that all reservoir outflow goes through the turbines unless installed capacity is exceeded, that is, $Q_{t,turb} = Q_{t,out}$. For all other plants, the turbine release is assumed to be equal to the WaterGAP 2.2d gridded streamflow time series, that is, $Q_{t,turb} = Q_t$.

Estimation of hydraulic head H_t also differs between the two plant groups but does not distinguish run-of-river plants from those reservoir-storage plants that are not among the 693 plants for which WaterGAP explicitly simulates reservoir storage. H_t is determined in two steps (Figure 2). In step 1, maximum hydraulic head H_{max} is set and in step 2, H_t. If H_{max} is available for a plant in GHD, we used this value directly. Otherwise, if H_{dam} is available, we assume

$$H_{max} = 0.92 H_{dam} \tag{2}$$

Dam freeboard (the safety margin for maximum water storage in the reservoir) is usually 4%–5% of dam height (Ali et al., 2012) and an equally tailrace water height was assumed. If there is neither a H_{max} nor a H_{dam} record, a multiple linear regression model was set up to estimate H_{dam} from GHD attributes of installed capacity of plant, gridded elevation difference H_{ele}, and long-term mean highest and lowest monthly streamflow of the grid cell in which the power plant is located. Visual inspection revealed no evidence of multicollinearity among these predictors. The regression model was first fitted for the 4,169 plants with observations of dam/weir height in GHD (correlation coefficient of this model $r = 0.6$ after removing outliers with studentized residuals that were larger than 3 in absolute value) and then used to assess the dam height for the remaining plants. Due to the low correlation, the minimum value of simulated dam height is set to 2 m, and for plants with installed capacity lower than 100 MW, H_{dam} was not allowed to exceed 200 m. The values of three predictors and estimated H_{dam} are all listed in GHD.

In case of the 693 WaterGAP reservoir plants, H_t is assumed to vary from month to month as a function of reservoir storage, with

$$H_t = H_{max}\left(\frac{S_t}{S_{max}}\right)^{\beta} \tag{3}$$

where S_t is WaterGAP 2.2d simulated monthly reservoir storage (10^6 m^3), S_{max} is the maximum reservoir storage (listed in GHD) (10^6 m^3), and $\beta = 0.9229$ is a regression parameter that relates storage variations to head variations and is taken from the GRanD technical document (Beames et al., 2019). For plants whose reservoirs are not in the WaterGAP simulation, they are implicitly treated as run-of-river plants. H_t is assumed to be temporally constant, with

$$H_t = \gamma H_{max} \tag{4}$$

where $\gamma = 0.68$ is a globally homogeneous calibrated parameter such that the simulated global gross HP in 2016 is proportional to the EIA statistic, taking into consideration of installed capacity coverage included in GHD.

For any single hydropower plant, the actual time series of electricity generation depends on the operation status of plants. When a plant is reported to be first commissioned/opened from a specific year (see Table 1, i.e., attribute Year_Open in Table S2), we then started to estimate the HP at the plant level. If this attribute is missing, we assume that this plant has already been commissioned before year 1975, which is the starting point of our simulation period. The operation status of plant can vary by time period due to maintenance, decommission, and accidental destruction (i.e., attribute Timeline in Table S2), we excluded the electricity generation during these nonworking years. The HP from plants that were still under refurbishment in 2016 or have been decommissioned/shutdown before 2016 was also excluded. Therefore, the monthly HP to the plant levels that were operational during the time period 1975–2016 was determined.

Changes in HP are mainly due to commissioning and decommissioning of hydropower plants and hydrological variability, and HP data, for example, annual HP country values from EIA reflect both influences. To decompose the effects of their changes, three model variants of model output V0, V1, and V2 were

Table 2
Description of the Reference HP Model Variants

Variant	Description	Streamflow and storage	Operating hydropower plants
V0	Baseline HP	Simulated historical series	Temporally variable
V1	HP assuming a constant number of plants	Simulated historical series	Plants existing in 2016
V2	HP assuming no interannual hydrological variability	Monthly mean	Temporally variable

simulated for the period 1975–2016 (Table 2): V0 takes into account the annually changing number of actually operating plants and the historical time series of hydrological inputs (i.e., Q_t, $Q_{t,out}$, and S_t). For V1, the historical hydrological inputs are applied for the hydropower plants existing in 2016, while in V2, 1975–2016 mean streamflow and storage values per calendar month are applied for the annually changing number of hydropower plants of V0. In other words, variant V1 assumes a constant number of operating plants while variant V2 assumes no interannual variability in the hydraulic head and turbine release. Annual HP time series from all the three variants were used in the following sections.

2.4. Evaluation Metrics

Three metrics, Nash–Sutcliffe efficiency (*NSE*) (Nash & Sutcliffe, 1970), coefficient of determination (R^2), and variability ratio (*CVR*) (Kling et al., 2012), are adopted to evaluate the performance of simulated time series (e.g., HP and streamflow). *NSE* and R^2 are traditional metrics in hydrological modeling. Along with the *CVR*, these metrics provide an integrated measure of modeling performance with respect to different components, that is, correlation, bias, and variability, respectively.

$$NSE = 1 - \frac{\sum_t (O_t - S_t)^2}{\sum_t (O_t - \mu_O)^2} \tag{5}$$

$$R^2 = \left(\frac{\sum_t (O_t - \mu_O)(S_t - \mu_S)}{\sqrt{\sum_t (O_t - \mu_O)^2 \sum_t (S_t - \mu_S)^2}} \right)^2 \tag{6}$$

$$CVR = \frac{CV_S}{CV_O} = \frac{\sigma_S / \mu_S}{\sigma_O / \mu_O} \tag{7}$$

where O_t is observed value (e.g., monthly HP), S_t is simulated value, μ represents mean value, σ is standard deviation, and CV is coefficient of variation. Ideal values for all the three metrics are 1, representing a perfect match of simulated series to the observed data.

2.5. Quantifying Streamflow Drought Hazard

2.5.1. Indicator of Streamflow Drought Hazard

To quantify streamflow drought hazard, we used the standardized streamflow index (SSI, Vicente-Serrano et al., 2011). Both mean and standard deviations for the 12 calendar months were computed over a reference period, here 1975–2016. In this study, we selected a 3-month accumulation period and analyzed SSI3 to focus the analysis on longer streamflow deficits and make model uncertainties, in particular, regarding the operation of reservoir that may lead to seasonal shift less impacting. To compute SSI3 for each month and 0.5° grid cell during 1975–2016, monthly WaterGAP 2.2d streamflow was first averaged over the last 3 months for each grid cell. Then, these 42 streamflow values (1975–2016) for each calendar month were fitted to a Pearson type III distribution (see Section S2 for the probability distribution test) and finally transformed to a normal distribution via the associated cumulative probability, resulting the SSI3. The SSI3

of -1 indicates the streamflow averaged over the last 3 months was one standard deviation lower than normal (i.e., the mean) for the respective three calendar months.

2.5.2. Three-Dimensional Streamflow Drought Event Identification

As droughts are regional phenomena, it is of interest to quantify drought hazard not only for individual 0.5° grid cell but to also identify large, spatially and temporally contiguous drought patches/events, and characterize them by their spatial extent, duration, severity, and intensity (Andreadis et al., 2005; Dracup et al., 1980). Using the approach proposed by Haslinger and Blöschl (2017), we performed the following four main steps.

(1) Identify the grid cells that are "under drought". Following Agnew (2000), a drought is assumed to occur if SSI3 is less -0.84, which occurs on average once every 5 years (corresponding to an annual probability of nonexceedance F of 0.2). Each F of each SSI3 value smaller than -0.84 is then mapped to the interval [0,1], with

$$q_{int,t} = \frac{0.2 - F\left(\text{SSI3}_t\right)}{0.2} \tag{8}$$

where F is the nonexceedance probability of SSI3 in period t. All grid points with positive $q_{int,t}$ for at least two consecutive months are considered as "under drought" in a temporal dimension of each 0.5° grid cell.

(2) Detect the spatial extent of drought. The 0.5° cells under drought are aggregated into different drought patches by searching their 3×3 neighborhood grids. Once a continuous drought area exceeds a threshold of 25,000 km^2 (around nine grid cells in the equatorial regions), it is considered as a drought event with reasonable size and therefore impact (Liu et al., 2019). With this approach, smaller drought patches are filtered out. In our study, only 13% of all grid cells and months, for which a positive $q_{int,t}$ was determined throughout the study period, were identified to belong to such reasonable large drought patches.

(3) Determine the temporal connection between drought patches. Because one single drought event in a month can break up into multiple smaller drought events, or several small droughts merge into one spatially larger event in the subsequent month, we assume that the drought patches in two consecutive months belong to one drought event if drought area overlap is larger than 50% of the area of the smaller patch while the denominator itself is no less than one quarter of the area of the larger patch.

(4) Extract drought features. The duration of the three-dimensional drought event is defined as the months between earliest initial and latest terminal time steps of all related grid points in the same event. For every time step, the monthly intensity is calculated as the sum of the gridded $q_{int,t}$ of the current drought patch. Drought severity is the cumulative monthly intensity over the whole drought duration, with

$$severity_{3d} = \sum_{t=s_{3d}}^{l_{3d}} \sum_{cell_t} q_{int,t} \tag{9}$$

where s_{3d} and l_{3d} are the initiation and termination periods of the three-dimensional drought event; $cell_t$ indicates all grid cells of the drought patch in period t.

2.6. Risk Analysis of Streamflow and HP Reductions

The risk analysis relates the severity of streamflow or HP reduction during a deficit event to its frequency or probability of occurrence. Different from Section 2.5, the deficit event is defined for either individual 0.5° grid cells or whole countries, that is, the sum of all grid cells pertaining to a country. Risks were computed with model variant V1, assuming hydropower plants that existed in 2016 and taking into account monthly values of streamflow and HP during 1975–2016. Both streamflow and HP deficits were derived as compared to the respective long-term mean at each grid, and then the deficit events were ranked according to their severity. A probability distribution was fitted to the ranked severity series to estimate the probability of exceedance of deficit events of a certain severity.

For the same reasons as for aggregating streamflow over 3 months (Section 2.5.1), we averaged also HP, for each month in the historical period, over the last 3 months to obtain HP3. For a specific hydropower plant, HP deficit Def_t occurs in months where HP3 is less than long-term mean over the same months ($\overline{HP3}$) for each plant, with

$$Def_t = \begin{cases} \overline{Var3_t} - Var3_t \text{ if } Var3_t < \overline{Var3_t} \\ 0 \quad \text{others} \end{cases} \tag{10}$$

The symbol Var stands for either HP or streamflow. In case of streamflow, the deficit computation was done per grid cell. For HP risk analyses at the grid cell level and country level, HP3 of each plant within a grid cell or a country was first added to the grid/national total HP3 before applying Equation 10. This aggregation is reasonable for hydropower because HP produced by individual plant is distributed via regional power transmission networks. Deficit events may last for a few months to multiple years. Severity of each identified deficit event was calculated as the sum of the monthly deficits over the event duration as

$$Sev(Var)_i = \sum_{t=s_i}^{l_i} Def_t \tag{11}$$

where s_i and l_i are the first and last time steps of a streamflow or HP deficit event i. In case of HP, it quantifies the amount of hydroelectricity that could not be produced due to dryer than normal conditions.

Each deficit event can be described by the probability that its severity is exceeded, applying the threshold method used for flood frequency analysis (Smith, 1984). The severities of all identified deficit events were ranked based on their magnitudes. Subsequently, a lognormal distribution was fitted to the top 42 streamflow severity values while Pareto type II distribution to HP severity values in the 42 years of 1975–2016 (see Section S2 for the distribution test). This step was to estimate the probability that in any year a streamflow/HP deficit event occurs that does not exceed a given severity. If there were less than 42 historical deficit events, the remaining events were fill by 0, representing ignorable severity of the deficit event. Streamflow/HP reduction during one event was expressed in terms of the severity value divided by mean annual streamflow/HP, with

$$Red(Var)_i = \frac{Sev(Var)_i}{Var_{annual}} \tag{12}$$

3. Results

In Section 3.1, we test the quality of the new GHD regarding its completeness by comparing the included installed capacities to independent country values. Computed annual time series of HP per country are evaluated against independent historical time series in Section 3.2. In Sections 3.3 and 3.4, we evaluate the performance of simulated streamflow drought and the drought impact on HP. Building upon these validations, the HP reduction during large contiguous droughts is assessed in Section 3.5, while the 1-in-10 year risk of HP reduction in individual grid cells or countries is presented in Section 3.6.

3.1. Completeness of GHD

Figure 3 compares the total installed capacity in 2016 in GDH to the statistics of EIA (2019) at the country level, for 134 countries. The six world regions are divided according to the International Hydropower Association regional classification (IHA, 2018). For 80% (i.e., 107) of the 134 countries, the differences in conventional installed capacities between EIA and GHD are within 10% or 0.1 GW. The largest absolute discrepancy is found for China, where GHD misses 23.5% of the EIA installed capacity (Figure 3a, the highest green symbol shown refers to China). Countries with relative discrepancy higher than 50% are found equipped with EIA installed capacities of less than 0.2 GW. Figure 3a also reveals that most countries in Africa hold conventional installed capacities of up to only 1.0 GW, while the opposite is true in the other five regions. The 10 countries with the top conventional installed capacities are, in descending order, China, Brazil, Canada, United States, Russia, India, Norway, Turkey, Japan, and France. Although this study does
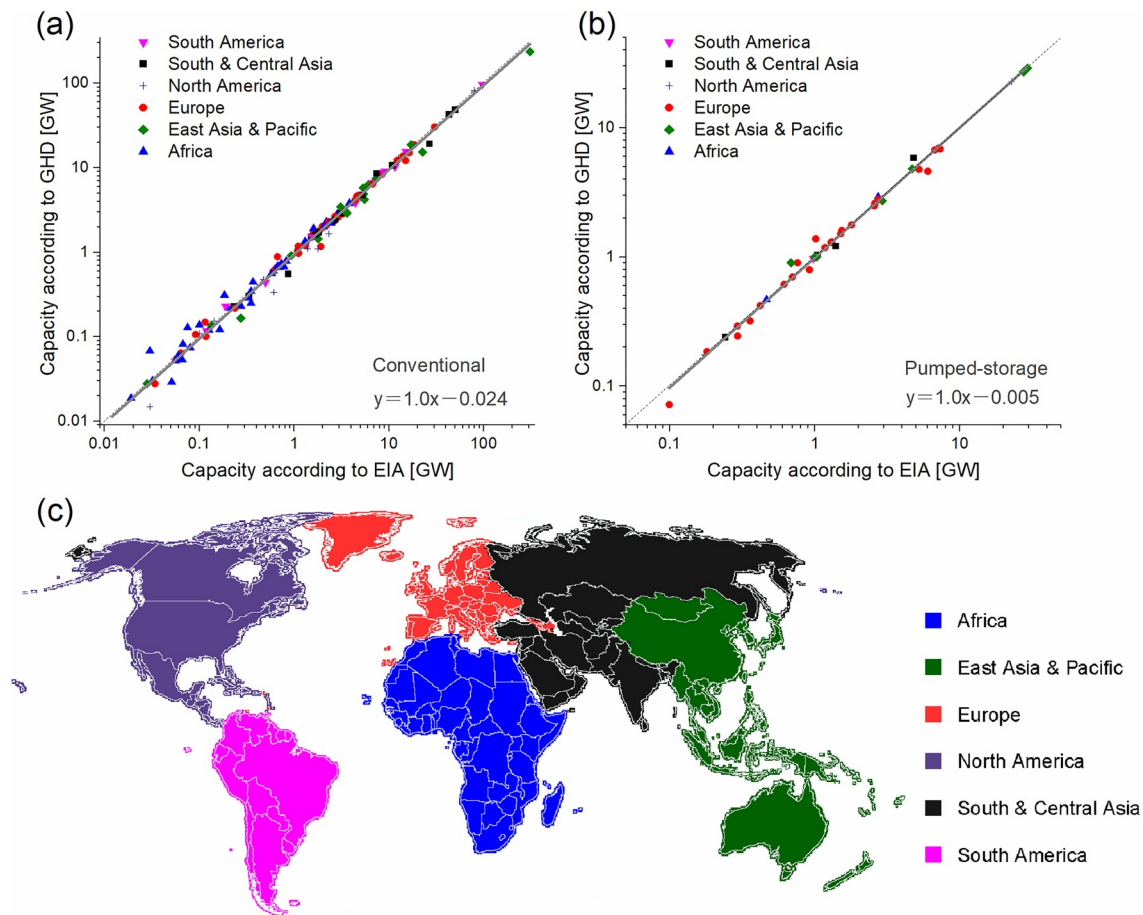
Figure 3. Comparison of country-level total installed hydropower capacity between EIA and GHD for the year 2016 distinguishing conventional (reservoir-storage and run-of-river) plants (a) and pumped-storage plants (b). The countries are categorized into six world regions according to IHA (2018) (c). Dashed lines in (a and b) represent 1:1 relationship, and solid ones are the linear regression curves (R^2 =0.99 in both cases). GHD, global hydropower database.

not consider the power production generated by pumped-storage plants, the GHD does include 288 records for pumped-storage hydropower. Merely, 41 out of 134 countries have pumped-storage plants and the largest two countries are in East Asia, that is, China (29 GW) and Japan (27 GW) (Figure 3b). On average, the linear relationship indicates a good hydropower plant coverage by GHD, indicating the reliability of GHD in terms of installed capacities and spatial distribution and its suitability for studying HP at the global scale.

3.2. Performance of Simulated Annual HP at the Global Scale

For a global-scale validation of the HP model, only annual time series of HP per country were available by EIA starting from 1980 (EIA, 2019). Figure 4 shows the *NSE* coefficient, coefficient of determination (R^2), and variability ratio (*CVR*) between simulated annual HP (using model variant V0) and EIA data for 1980–2016. In general, the metrics vary strongly among countries. *NSE* and R^2 are relatively low in Africa, with 27 out of 38 countries having negative *NSE* and 22 with R^2 of less than 0.5. The unsatisfactory performance in Africa is partly due to the unsatisfactory simulation of streamflow of WaterGAP in this region (Müller Schmied et al., 2021). The sparse distribution of hydropower plants and small quantities of total installed capacity in African countries is another reason. Around half of the countries, especially the large ones, have positive *NSE* (43% of the countries), $R^2 \geq 0.5$ (57%), and a *CVR* in the range of [0.7,1.4] (66%). Countries with high overall performance (i.e., $NSE \cdot R^2 / |CVR - 1| > 1$, 28%) include China, Brazil, Canada, United States, India, France, Spain, and Sudan (listed in the order of total installed capacity). For many countries,
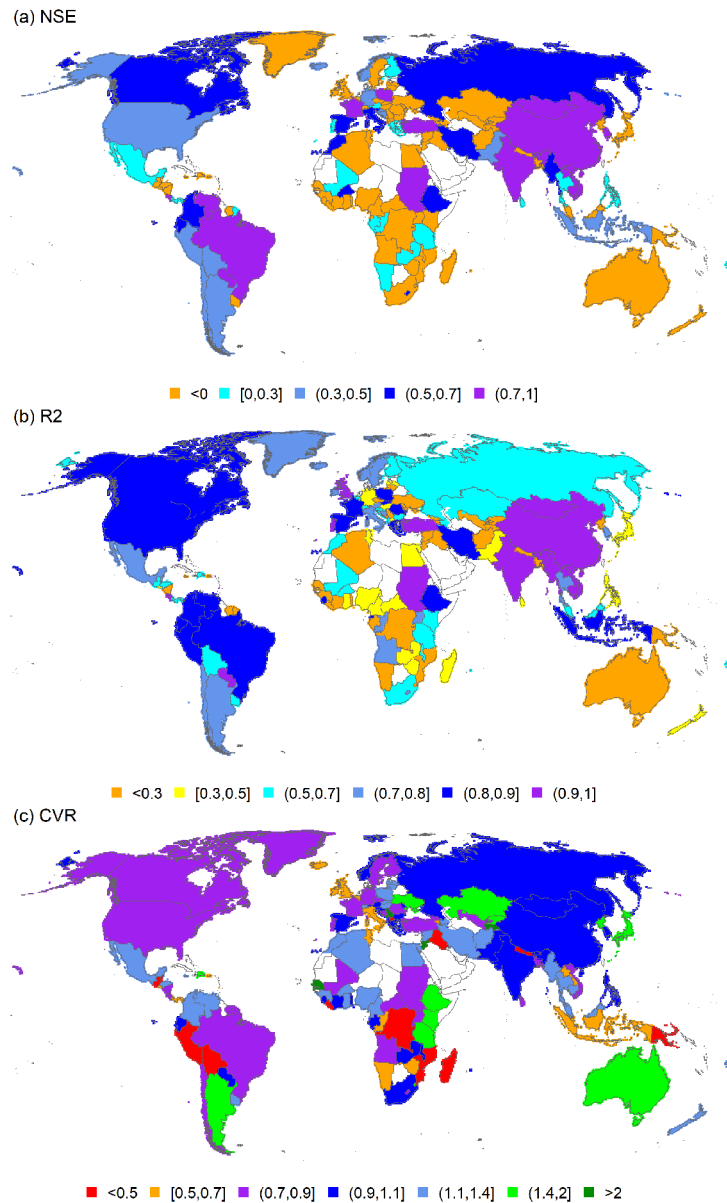
Figure 4. Performance of annual HP series represented by Nash–Sutcliffe efficiency (*NSE*) (a), coefficient of determination (R^2) (b), and coefficient of variation ratio between the simulated values and EIA data (*CVR*) (c) over the period 1980–2016 for countries equipped with conventional power plants. HP, hydroelectricity production.

the annual time series are dominated by a strong upward trend due to an increasing number of hydropower stations (e.g., China and India, Figure S1), not by climatic variations.

Figure 5 presents a comparison of the simulated and statistical annual time series of HP (V0) for all plants within the six world regions. The statistical data are well captured by the HP simulation, except for the region East Asia and Pacific. The latter is due to the incomplete records on installation of new hydropower plant, particularly in China, which contributes most to the overall rapid increase behavior of regional HP (Figure S1a). The observed interannual variabilities in Europe and North America are simulated well by the HP model (Figure 5). In case of Africa, however, statistics do not support the international variations around the trend that is simulated. In the other three world regions, the annual time series are dominated by upward trends.
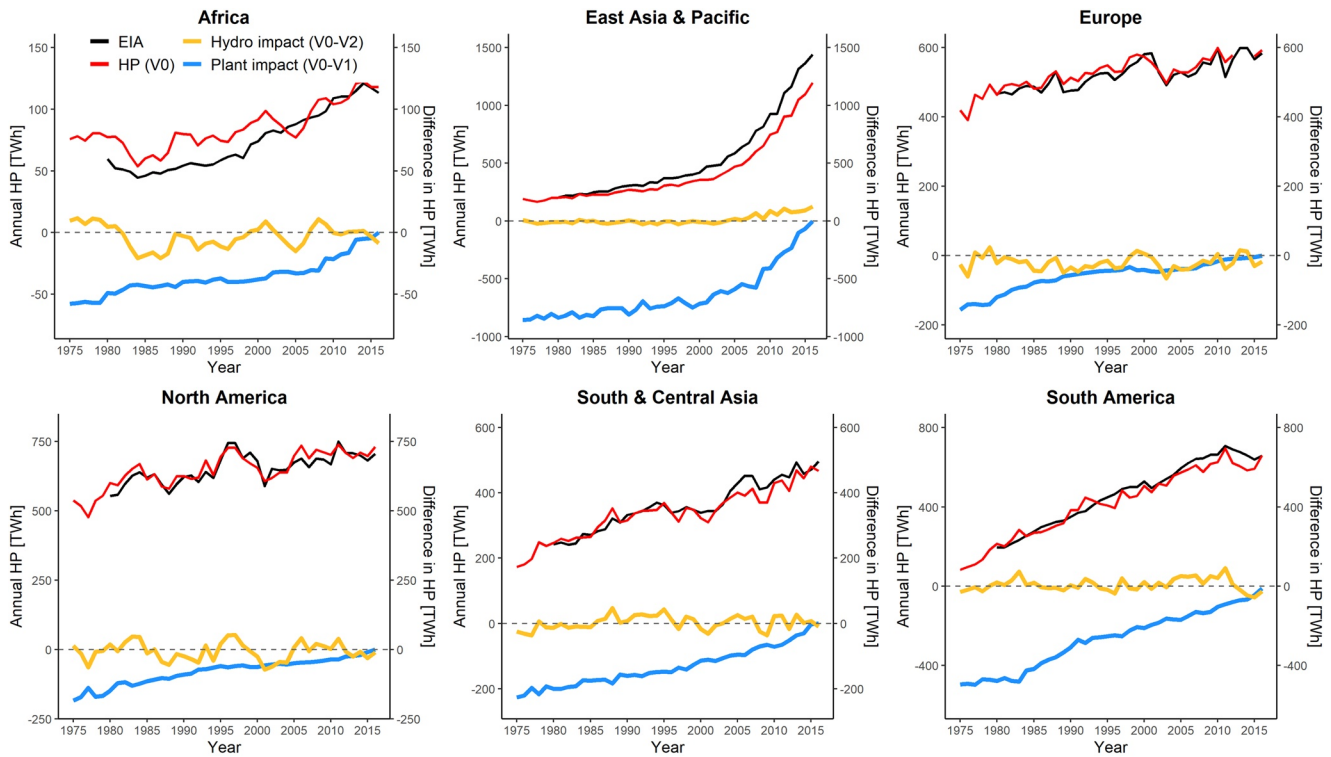
Figure 5. Series of long-term annual HP and HP differences for the six world regions during 1975–2016. Red lines show the simulated HP (V0), black lines EIA statistics (1980–2016). Gold lines represent the impact of hydrological variability (difference between V0 and V2, the latter assuming mean monthly streamflow and reservoir storage) on simulated HP, blue lines the impact of plant variability (difference between V0 and V1, the latter assuming that the 2016 plants existed throughout the simulation). HP, hydroelectricity production.

Figure 5 also shows the results of decomposing the HP (V0) time series obtained considering climate variability and the changing number of hydropower plants into the impact of hydrological variability (gold lines) and of plant variability (blue lines). The positive trends of plant-impact lines in all six regions are due to increasing values of total installed capacities. The occasional fluctuations suggest the unexpected shutdown or decommissioning of some large plants in those specific years.

The hydro-impact lines do not show any significant trends but large variations around the zero due to the interannual variability of streamflow, with negative values (of differences between the HP simulation with historical streamflow/storage and the simulation with long-term mean monthly streamflow/storage, see Table 2) indicating unusually dry years. For example, Africa witnessed two obvious HP depressions in 1982–1988 and 2002–2006, which coincide with the reported extreme droughts in Africa (Masih et al., 2014). Equally, the large North America droughts around 1977, 1988, and 2002 (Andreadis et al., 2005) are also reflected in the HP simulation. The mean values of the hydro-impact curves were calculated. It is found that only regions of East Asia and Pacific, South and Central Asia, and South America have negative values, which indicates a higher HP of V2 than of V0 in the long run. In the other three regions, the reverse is true. Theoretically, for hydropower plants without WaterGAP reservoir simulation, the mean monthly streamflow/storage variant (V2) should result in more or at least the same HP as variant V0 because of less high flow losses due to the installed capacity constraint. However, for the WaterGAP reservoir plants, the assumption in variant V2 may conversely decrease HP because of the existence of the complementary effect between release and storage, that is, per unit release becomes more productive as storage increases (Zhao et al., 2014). For instance, consider two periods, when in period t_1 both turbine release and hydraulic head equal 1, and in period t_2 equal 3, then the total HP is $10\eta\Delta t$ according to Equation 1. Assuming mean release and storage of 2 as in the case of V2, the total HP becomes $8\eta\Delta t$.
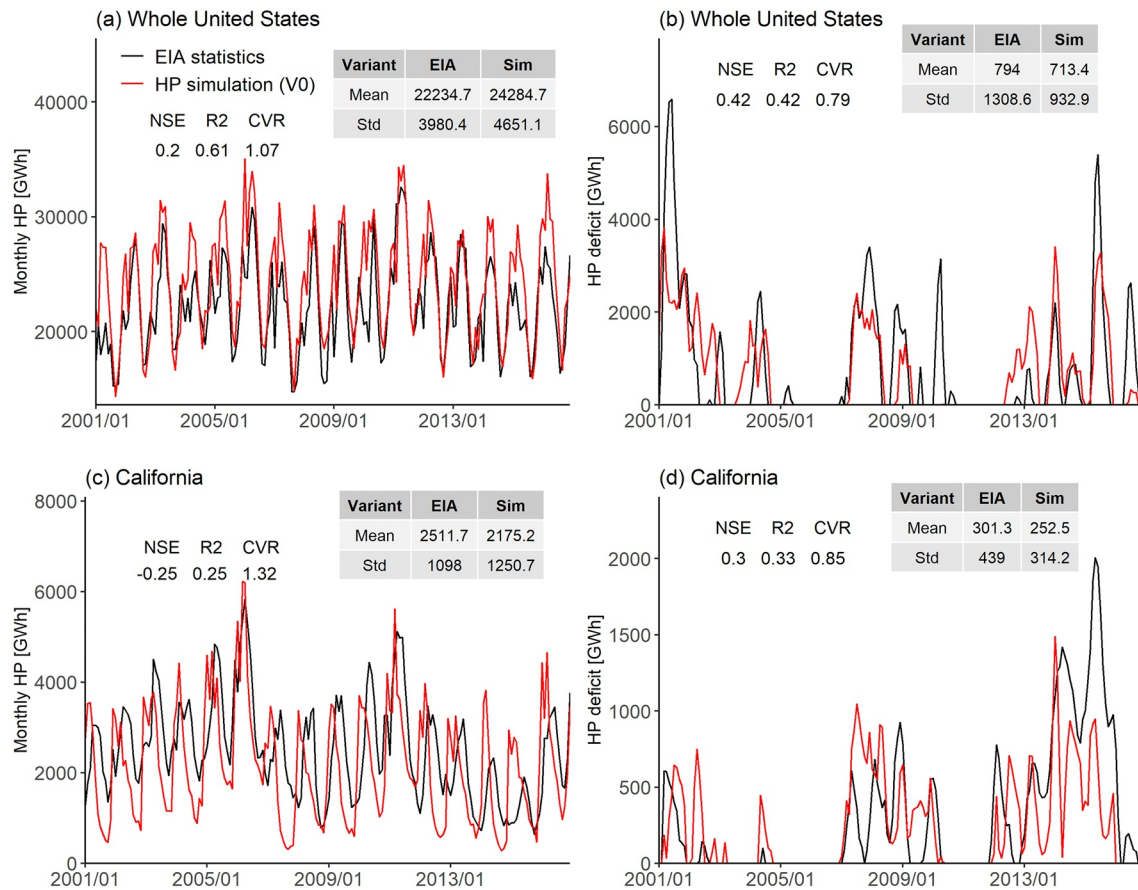
Figure 6. Monthly net generation of conventional hydropower and HP deficit for the United States (a and b) and the state of California (c and d) in 2001–2016. Comparison between EIA statistics and HP simulated by model variant V0. HP, hydroelectricity production.

3.3. Performance of Streamflow Drought Simulation

Simulation of streamflow drought impact relies on a reliable simulation of streamflow and in particular streamflow drought. Performance of WaterGAP with respect to streamflow has already been extensively discussed (e.g., Müller Schmied et al., 2014, 2021; Zaherpour et al., 2018). Therefore, we tested the performance of streamflow drought simulation as indicated by standardized streamflow index (SSI3) against observations at 183 stations (Figure S2) worldwide for which continuous time series of monthly streamflow were available during 1971–2000 (more details are provided in Section S4). The observed streamflow was provided by Global Data Runoff Centre. The agreement of *NSE* for SSI3 was moderate with a median of 0.5 and an interquartile range between 0.2 and 0.7 (Figure S3). The goodness-of-fit for streamflow is very similar, albeit with slightly lower quartile of 0.14. At 25 stations (41% of assessed basin area), both *NSE*s exceeded 0.7. At a large number of stations (83% of assessed basin area), simulated and observed SSI3 values were classified into the same drought hazard class in 70% of the time (Figure S4).

3.4. Performance of Simulation of Drought Impact on HP

3.4.1. Monthly HP in the US

To test the capability of the HP model for simulating drought impact on HP, one would ideally compare simulation results at spatial scales below the country scale and temporal scales below the annual. However, such data are not available globally. We therefore evaluated data on monthly HP in the federal states of the US that are available from January 2001 (EIA, 2019). Figure 6 shows the comparison of time series of simulated monthly HP (V0) for the whole US and the state of California as compared to the EIA statistics. In the US, seasonality and interannual variability of HP are represented quite well by the model, with HP rising

in late winter and dropping in late summer, recognizable difference between wet and dry years (Figure 6a). Both the statistical and simulated HP deficit series (see Equation 10 in Section 2.6) in the period 2001–2016 reveal three major drought events in 2001–2002, 2007–2009, and 2012–2016 (Figure 6b). The simulated mean HP deficit of 713 GWh is close to the observed value of 794 GWh.

The 2007–2009 and 2012–2016 droughts struck large parts of California. In 2016, hydropower in California represented 13.7% of the national total installed capacity, with conventional plants of 10.2 GW and pumped-storage plants of 3.9 GW in GHD; this composition has remained almost constant since 1990. The HP model overestimates seasonal variability and underestimates the seasonal low values (Figure 6c). This may be due to the artificial water transfers into California that are not taken into account by WaterGAP. The HP model reproduces the observed HP deficit (Figure 6d) much better than the HP itself. This makes sense because the HP deficits are relative values after removing seasonality. Initiation and termination of HP deficit events almost coincide with that obtained from EIA statistics. During the most recent two multiyear droughts, HP is observed substantially below average, and the cumulative HP reductions (severity as defined in Equation 11) are 18.2 TWh simulated versus 12.6 TWh observed and 22.8 TWh simulated versus 41.5 TWh observed for the 2007–2009 drought and the 2011–2016 drought, respectively. Evidently, HP reduction during the 2011–2016 drought is strongly underestimated, especially after March 2014. Water flows in particular in southern California are heavily managed, and it is likely that water allocation for households and irrigation was increased during later stages of drought.

3.4.2. Analysis of HP Reduction During the 2003 Central European Drought

To reveal how streamflow drought influences HP at the country scale, we took the 2003 European drought, focusing on the Central European countries (hereinafter referred to as 2003 CEU drought, Figure 7a). The 2003 CEU drought was classified as a 30-year drought, that is, a drought with a return period of 30 years, based on temperature data (Charpentier, 2011). According to the three-dimensional drought event identification method explained in Section 2.5, the 2003 CEU drought began in early spring (February 2003) and intensified from June, then rapidly expanded to cover 75% area of Central Europe in August. The drought began to quickly recede in October and completely disappeared in March 2004 (Figure 7b). The grid-level drought duration (see Equation 8) was found the longest in Poland, where most grids were under drought for more than 8 months (Figure 7a). Central north Germany and eastern Hungary were least affected, with some grid cells without any negative streamflow anomalies.

Due to the low precipitation and extremely high temperature and thus low streamflow, the energy sector was challenged by a reduced potential of hydropower (Mukheibir, 2013). In CEU, most plants are concentrated in the south in Switzerland (CH), Austria (AT), Czech Republic (CZ), and Slovakia (SK) (Figure 7c). The time series of annual HP (V0) over CEU simulates well the strong interannual variability of HP shown by the EIA statistics, with years of high HP such as 1993 and 2013 and years of low HP such as 1996, 1997, and 2010 being reproduced (Figure 7d). However, the HP reduction in the drought year 2003 (but not in 2015) is strongly overestimated by the HP model. Compared to 1980–2016, the simulated HP reduction is 11.8%, while according to EIA it is only 4.0%. Considering the CEU drought period February 2003 to March 2004, HP was reduced by 11.4% with respect to 1980–2016. The overestimation of drought impact in CEU during 2003 as compared to EIA statistics is due to an overestimation of HP reduction for two HP producers, Switzerland and Germany (Figures 7e and S6a, compare red triangles to black circles for country-scale relative anomalies). In both countries, the HP value according to the statistics was very close to normal. The simulated HP (V0) anomalies are quite consistent with the statistics in Austria (AT), the country with the second highest installed capacity, Slovakia (SK), Czech Republic (CZ), and Hungary (HU) and relatively close in Slovenia (SL).

To isolate the drought impact on HP reduction, HP during the drought period should not be compared to the time series of actual HP within any spatial unit as this includes the impact of the number of active plants on HP. Evaluation of the V1 runs, with a constant distribution of hydropower plants, resulting in larger reductions from normal conditions during 2003 (Figures 7f and S6b). All counties, except Czech Republic, are simulated to suffer reductions of more than 15%, or around 1.0–2.0σ.
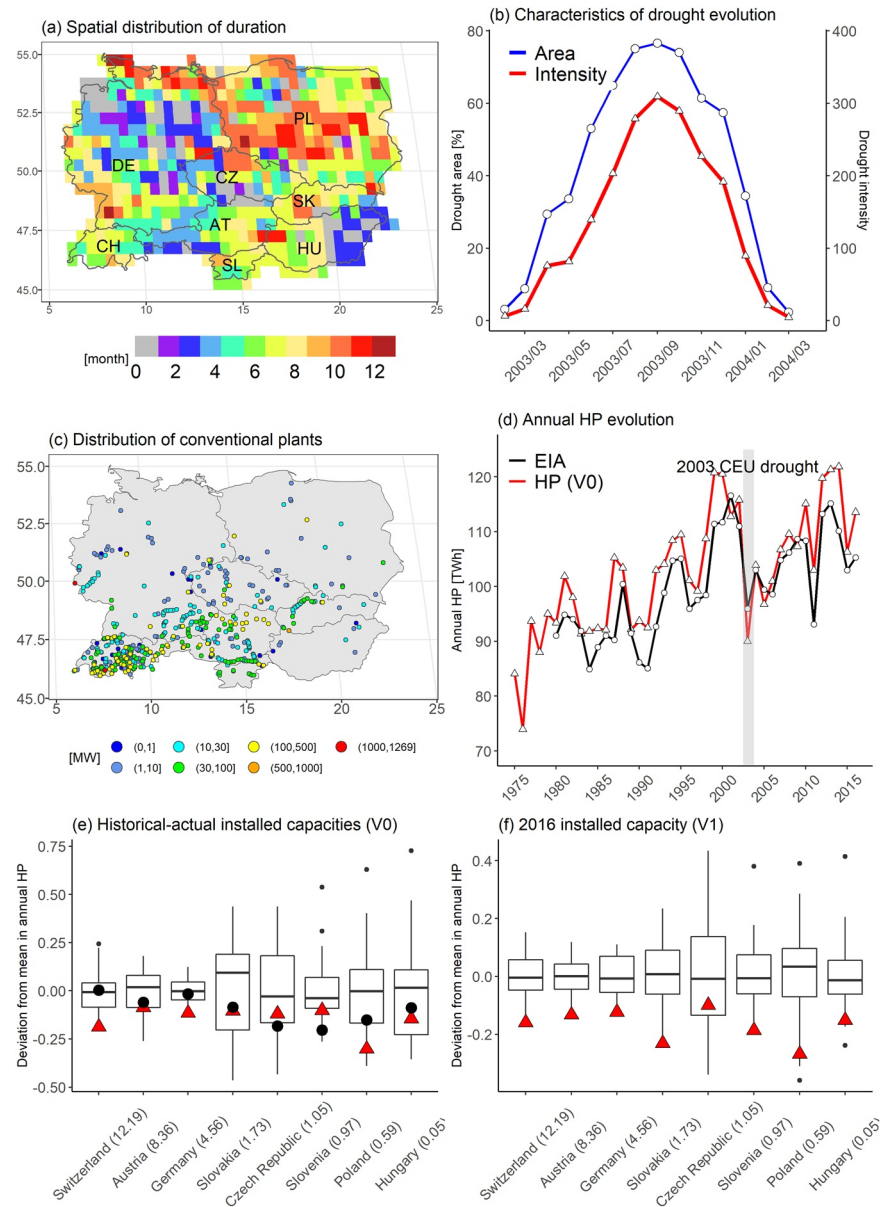
Figure 7. Spatial–temporal evolution of 2003 CEU streamflow drought in terms of grid-level drought duration in month (a), and three-dimensional drought intensity and areal coverage (% of CEU area) (b); spatial distribution of conventional hydropower plants with installed capacity (c), and simulated annual total HP (V0) in CEU as compared to EIA statistics for 1980–2016 (d); box-plot for HP (V0, based on time-varying hydropower plants) and HP (V1, based on 2016 hydropower plants) showing the simulated relative deviations in 2003 from the long-term mean annual HP over 1980–2016 with the respective country as a whole (e and f). Countries are ordered by installed capacity in GW (in parentheses after country name) as included in (c). The filled red triangles in (e and f) are the simulated mean relative deviations in year 2003, and filled black circles in (e) are derived from EIA statistics. HP, hydroelectricity production.

3.5. HP Reduction During Large Contiguous Droughts

Globally, a total of 14,641 large contiguous drought events with a minimum extent of more than 25,000 km^2 have been identified in the period 1975–2016 using the method explained in Section 2.5. During these 42 years, several prolonged as well as widespread droughts have occurred. Table 3 summarizes the drought characteristics of the 20 most notable events in terms of severity, which are in agreement with the major drought events reported in the literature (Bonsal et al., 2011; Masih et al., 2014; Spinoni et al., 2015; Zhang

Table 3
Twenty Most Severe Streamflow Drought Events Affecting a Large Contiguous Region Over a Long Time Period, Ranked by Severity According to the Definition Described in Equation 9 in 2.5.2

Rank	Affected region	Period	Duration (month)	Severity	HP reduction (V1) (%)	$N_{installed}$ coverage (%)
1	Europe	04.1975–08.1977	29	41,661	13.4	15.9
2	Central Russia	12.1984–03.1988	40	32,887	24.1	1.1
3	Sahel region of Africa	07.1981–08.1987	74	30,813	20.4	1.1
4	North America	12.1986–11.1992	72	23,999	6.1	10.9
5	North America	10.1995–10.2001	73	21,980	4.5	7.4
6	North America	05.1998–06.2003	62	21,121	1.1	5.8
7	Central Russia	06.1981–08.1983	27	21,116	18.1	3.2
8	Australia	07.1986–12.1991	66	18,530	1.4	0.1
9	Northern Canada	07.1994–08.1998	50	18,030	7.5	0.1
10	Northern Europe and Russia	01.1996–10.1997	22	16,756	10.3	11.3
11	East Asia, mainly China	07.2002–04.2005	34	15,807	5	10.9
12	Europe	02.2002–08.2005	43	15,719	4.2	14.8
13	Africa	01.2009–10.2011	34	15,175	10.1	1.2
14	South America	04.1997–10.1999	31	14,544	4.7	7.4
15	North America	05.2003–03.2005	23	14,337	9.2	7.3
16	South America	10.1991–02.1994	29	14,198	5	5.4
17	Russia	07.2011–04.2013	22	13,754	6.4	1
18	Europe	07.1983–04.1985	22	13,120	9.4	8
19	United States	12.2010–02.2015	51	13,036	6.9	4.6
20	South Asia	08.2000–11.2002	28	12,578	13.6	7.1

Note. A severity of 5,000 could be due to, for example, the existence of a drought patch with on average 1,000 cells with a 1-in-10 year drought occurrence ($q_{int,t}$= 0.5) over on average 10 months. HP reduction (V1) indicates the relative deviation from the mean monthly HP (V1, based on 2016 hydropower plants) over 1975–2016. $N_{installed}$ coverage refers to the installed capacity affected by the drought event in percent of the globally installed capacity in GHD in 2016.

& Zhou, 2015). From the listed events, areas of Northern Europe (and Russia) and North America show the highest number of drought events between the 1970s and 2010s, making up 13 of the top 20 severest events.
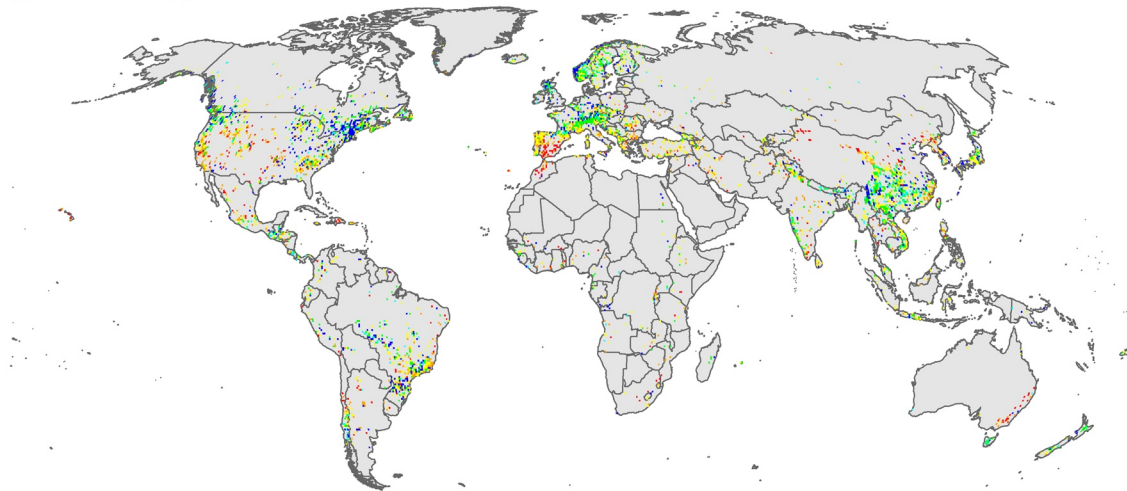
Among these top events, the 1976 European drought that occurred between April 1975 and August 1977 is ranked as the most severe one and lasted for 29 months. If the hydropower plants of the year 2016 existed during this drought (model variant V1), the simulated HP reduction would have been 13%. Hydropower in the drought-affected region accounted for 6% of worldwide installed hydropower capacity in 1977 and for 16% in 2016 (Table 3). Since 2000, Europe has witnessed a series of extreme dry events in combination with heatwaves, for example, 2003, 2010, and 2015 (Laaha et al., 2017; Schewe et al., 2019). The 2003 CEU drought presented in Section 3.4.2 is part of the detected 2003 European drought, which is ranked as the twelfth strongest drought event. It occurred from February 2002 to August 2005 and reached its peak in September 2003, with a total severity of 15,719 (Table 3).

The fifth strongest drought event originated from the Northwest Territories of Canada and gradually moved south to western America in the end of 2000; the sixth severest drought also began in Canada but the region of Central Canada and invaded much of the eastern and southern regions of the United States. The two extreme droughts together led to a tremendous HP deficit in the US in June 2001 of up to 25% (6.6 TWh) less HP compared to that of the corresponding period for the year 2001–2016, as shown in Figure 6b.

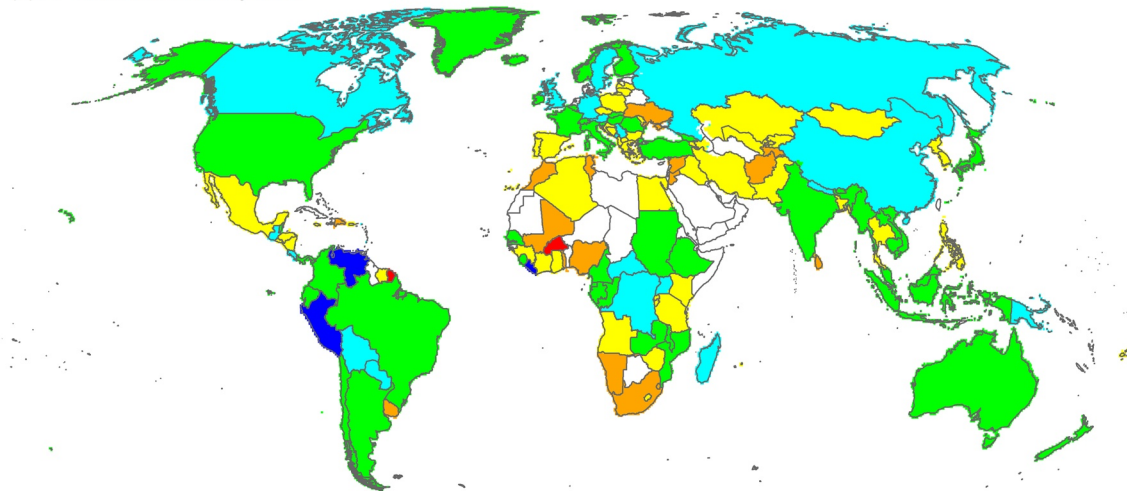### 3.6. Risk of HP Reduction due to Drought

Each plant, grid cell, or other spatial units is under a certain risk of HP reduction due to drought, which can be expressed as the probability that a certain reduction of normal annual HP is exceeded in each year or

(a) HP reduction, grid level

[%] ■ (0,5] ■ (5,10] ■ (10,20] ■ (20,40] ■ (40,70] ■ (70,100]

(b) HP reduction, country level

[%] ■ (0,5] ■ (5,10] ■ (10,20] ■ (20,40] ■ (40,70] ■ (70,100]

Figure 8. HP reduction in percent of mean annual HP that occurs in 1 out of every 10 years (i.e., with an annual probability of occurrence of 10%) at the grid level (a) and the country level (b), based on HP (V1) simulation for the period 1975–2016. HP, hydroelectricity production.

equivalently as the HP reduction that is exceeded with a certain probability or return period. Using model variant V1 considering hydropower plants existing in 2016 (Section 2.6), we computed, for 0.5° grid cells and whole countries, the HP reduction in percent of mean annual HP that is expected to be exceeded with a probability of 0.1 in any year or, equivalently, in 1 out of 10 years (Figure 8). A value of 20%, for example, means that, considering the streamflow variability during 1975–2016, there is a 10% chance in any year that this location faces a reduction of at least 20% of its mean annual HP (Equation 12). Under nonstationary conditions, which are mainly due to climate change, the values in Figure 8 are only an approximation also because historical streamflow time series can no longer be directly used to derive probabilities.

In 1 out of 10 years, 54% of all 4,082 grid cells containing power plants face an HP reduction of more than 20%. HP reduction is particularly high in semiarid areas, like the western United States and the Mediterranean region, unless hydropower plants are located on large rivers. In 7% of the cells, HP is even expected to be reduced, in 1 out of 10 years, by more than 70% as compared to mean annual HP. In contrast, there is almost no HP reduction in 18% of the cells (HP reduction $\leq$ 5%) when a 10-year HP deficit event occurs.

At the country level, HP reduction in 1 out of 10 years is between 3% in Venezuela and 79% in Burkina Faso (Figure 8b). China, accounting for 22% of global HP, shows a small HP reduction of only 8% even though many individual power plants are simulated to suffer from reduction of more than 10% or even 40% (Figure 8a). This is because (1) as a large country, if one region of the country suffers from a drought the other would not and vice versa, and (2) most of the large Chinese hydropower plants are subject to very low reductions of less than 5%. There are 67 out of 134 countries with relatively small HP reductions (≤20%), while 49 countries show moderate HP reductions between 20% and 40%, including countries in Central America and the Middle East. It appears that the majority of these moderately affected regions also have relatively low proportion of hydropower in energy ($r(HP)$ ≤0.3, Figure 1b). The 18 countries with high HP reductions of more than 40% are mostly found in Africa. Only two countries show more than 70% HP reduction, Burkina Faso (79%) and French Guiana (73%). In these countries, HP is not the dominant source of electricity. According to our study, total electricity production in 1 out of 10 years is only reduced by 11% and 36% in Burkina Faso and French Guiana, respectively. It is, rather, Togo whose total electricity production is calculated to be most strongly affected by streamflow drought. There is every year a 10% chance that total electricity production in Togo, which heavily relies on HP ($r(HP)$ = 0.87), is reduced by 55%.

4. Discussion

In Section 4.1, we discuss the uncertainties of global-scale HP simulation as presented in this paper. The relation between streamflow drought and HP reduction is analyzed in Section 4.2.

4.1. Uncertainties of Global-Scale Simulation of HP

Drought adaptation strategies, for example, modification of electricity prices and the demand-load portfolio, are not taken into account in the HP model. Therefore, actual reduction of HP during periods with streamflow deficits may be overestimated by the HP model. The HP model only simulates the direct impact of changes in streamflow or outflow from reservoirs on HP during periods of drought.

4.1.1. Uncertainty of Simulated Streamflow

An assessment of these direct impacts requires a good quantification of changes of flow during drought. A comparison to streamflow observations at 40 globally distributed gauging stations in eight hydrobelts showed that WaterGAP simulates the streamflow that is exceeded in 95% of all months very well, while annual 3-month low flows for different return periods are overestimated (Zaherpour et al., 2018). Our analysis of model performance specifically during drought conditions, comparing SSI3 indicators based on simulated and observed streamflow at 183 gauging stations, indicates that WaterGAP simulates reduction of streamflow during drought reasonably well (median *NSE* equals to 0.5, Section 3.3).

Furthermore, while anthropogenic alterations of streamflow by water use and reservoir operations are modeled in WaterGAP, in particular the simulation of the effect of reservoir operation on streamflow is very uncertain. The existence of reservoir modeling mostly improves model performance, yet the discrepancies between modeled and observed outflows remain high due to a variety of reasons, including uncertainty of simulated inflow and water use as well as of the assumed reservoir operation algorithm (Döll et al., 2009). Therefore, unfortunately even for the 693 WaterGAP reservoir hydropower plants that account for 35% of the global installed capacity of convention plants, the uncertainty related to the simulated turbine release, reservoir storage (Section S6) and thus HP is high.

We believe that mainly due to the uncertainty of the climate forcing, in particular of global data sets of precipitation, a higher temporal (daily) and spatial resolution of streamflow modeling would not increase the reliability of simulated streamflow. A 36-fold higher spatial resolution of WaterGAP (5 arc-minutes, approx. 9 km × 9 km at the equator) did not lead to an improved simulation of observed streamflow as compared to the 0.5° model version applied in this study (Eisner, 2016).

4.1.2. Uncertainty due to Operating Hours

A further simplification for global-scale simulation of HP was usage of aggregated monthly streamflow and H_t values. The HP model assumes that hydropower turbines run all day and night throughout the month
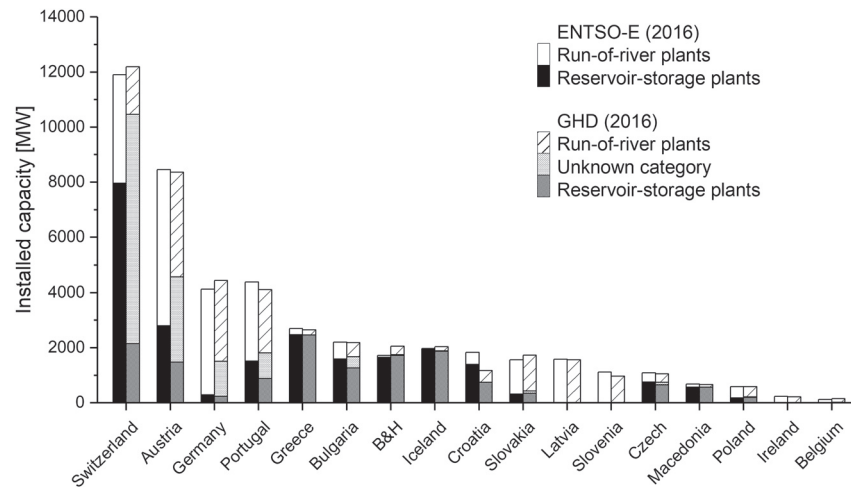
Figure 9. Comparison of conventional installed capacities for selected European countries between ENTSO-E statistics and the GHD database, distinguishing run-of-river and reservoir-storage plants as well as plants of unknown category. GHD, global hydropower database.

and that total streamflow is diverted into the power plant. In reality, hydropower plants rarely operate 24/7. The actual turbine release is not constant within a month. However, the load factor is not available for most hydropower plants. Only 36 large plants were equipped with the attribute of load factor (see Table 1) because (1) their data were relatively easily available and (2) the simulated HP of these plants was found to deviate significantly from the reported mean annual HP (i.e., attribute Gen_Gwhyr in Table S2) and thus substantially affects the country-level HP as compared to the EIA statistics due to their large installed capacities. To deal with these uncertainties, we (1) used the $N_{installed}$ as upper boundary of power output (see Equation 1) and (2) adopted a head reduction coefficient γ (see Equation 4) for a better fit to HP statistics, which partly reflects the load factor. As only relative changes in HP are analyzed in this study, the uncertainty due to flow and head deviations is believed to be within acceptable limits, as demonstrated in the case of California in Figure 6.

4.1.3. Uncertainty Regarding the Category of HP and the Incomplete Representation of Reservoir-Storage Plants

For almost half of the globally installed conventional capacity, there is no information in GHD on the plant category (Section 2.1), that is, is unknown whether the plant is a run-of-river plant without any control on the amount of water flowing through the turbine or a reservoir-storage plant with controlled release. 12.4% of the installed capacity is known to be related to run-of-river reservoirs (or pondages) and 42.1% to reservoir-storage reservoirs. In the HP model, only 35% of the installed conventional capacity (693 plant records) is located at WaterGAP reservoirs and is thus simulated with a temporally varying hydraulic head (Equation 3). Three hundred and sixteen of these 693 plant records are known to relate to reservoir-storage plants and 20 to run-of-river plants.

The question is what the likely category of the hydropower plants without information on category is. We have compared the total installed capacities of run-of-river and reservoir-storage plants in some European countries to ENTSO-E (2017) data, which provide the fraction of run-of-river and reservoir-storage installed capacity per country. In case of Switzerland, the majority of installed capacity without known category belongs to reservoir-storage plants, while in Austria and Germany, the majority belongs to run-of-river plants (Figure 9). It is therefore not possible to make general assumptions about the category of plants without known category.

Anyway, run-of-river plants can have a large fall (hydraulic head) and a quite large reservoir (even though low-head plants dominate). For example, the Fatschbach power plant (15 MW) in Switzerland produces electricity over a useable gradient of 578 m (Axpo, 2020), and the Chief Joseph Dam (2620 MW) in the United States, with a dam height of 72 m, is operated in a run-of-river mode (Yildiz & Vrugt, 2019).
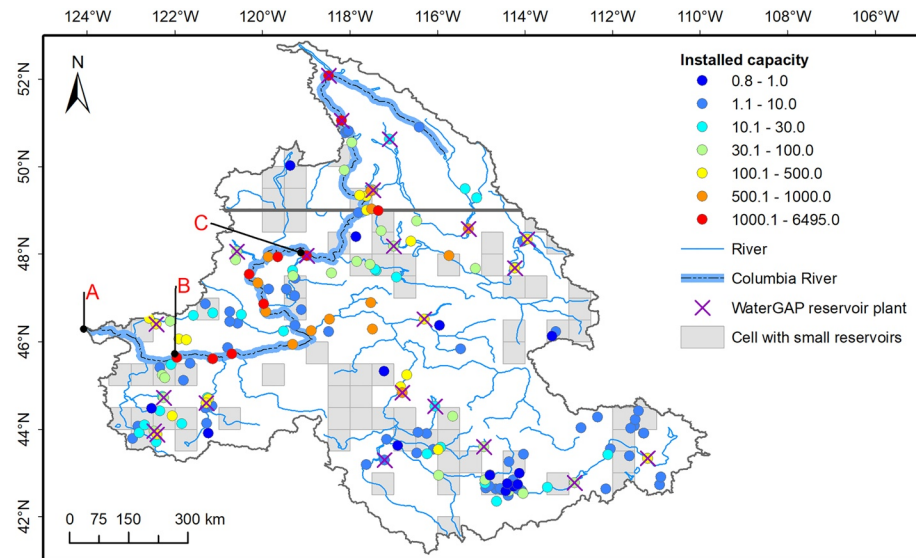
Figure 10. Distribution of the conventional hydropower plants and reservoirs in the Columbia River Basin according to the GHD. Grid cell A is the river mouth of basin into the Pacific Ocean, B is the cell where the plant with the largest catchment area is located, and C is the cell where the WaterGAP reservoir plant with the largest catchment area is located. GHD, global hydropower database.

The HP model does not distinguish simulation of run-of-river hydropower from reservoir-storage hydropower (Figure 2) which is an appropriate approach given the large fraction of hydropower plants without known category. However, even if there were more information on plant category available, this approach could not be changed because the WaterGAP model cannot simulate the water balance of individual small reservoirs that may be located at small tributaries whose streamflow cannot be resolved at the 0.5° grid cell resolution. It is therefore necessary to assume constant hydraulic heads H_t (Equation 4) for all reservoirs that are not located at large WaterGAP reservoirs that are assumed to be located at the river mainstem. WaterGAP does take into account 5000 small man-made reservoirs with a storage capacity below 0.5 km^3 (Müller Schmied et al., 2021) that are located in 32% of the cells with hydropower plants. However, these small reservoirs are aggregated with all small natural lakes within each grid cell and local runoff is routed through this aggregate water storage compartment, such that small reservoirs affect streamflow in the river mainstem, smoothing, and delaying streamflow from subscale tributaries. With an increased spatial resolution of WaterGAP, the number of reservoirs with an explicitly modeled water balance and thus the hydropower plants whose HP could be modeled as a function of reservoir storage (Equation 3) could be increased. However, given the difficulty to simulate very plant-specific operation rules by a globally applicable algorithm, it is expected to lead to very uncertain reservoir storage and thus H_t simulation.

The impact of constant H_t on simulated HP was tested by performing an additional simulation (hereinafter referred to as variant V3) where for all plants, including the plants located at WaterGAP reservoirs, a temporally constant H_t (Equation 4) was applied. The V3 simulation was run for the period 2001–2016 in the Columbia River Basin (CRB), which is located in the Pacific Northwest of North America (Figure 10). The CRB covers an area of 668,000 km^2. Two hundred and six conventional plants amounted to 39.8 GW in 2016, and only 27 of them, with an installed capacity of 15.4 GW (39% of basin total) and producing 25% of the total basin HP, are simulated as WaterGAP reservoir plants (purple cross in Figure 10). We found that the impact of constant H_t on mean and variability of HP and HP deficit strongly depends on the specific hydropower plants taken into account so that no general conclusions on the impact of this assumption on HP can be drawn.

4.1.4. Interpretation of the Simulated HP Bias in the US and CEU

A previous evaluation on 2003 European drought of Schewe et al. (2019) also claimed that their hydropower models constructed by Van Vliet, van Beek, et al. (2016), using VIC global hydrological model, mostly
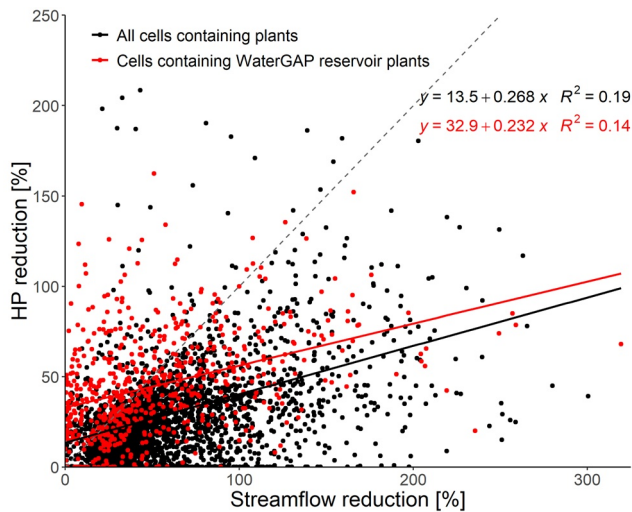
Figure 11. Scatter plot of streamflow and HP reductions (Equation 12) that occur in 1 out of 10 years at the grid cell level. The dashed line represents 1:1 relationship, and solid ones are the linear regression curves. HP, hydroelectricity production.

overestimate the drought impacts. However, the results in Section 3.4 reveal that this is not always the case. We assume that the deviations from the EIA statistics in the US and CEU lie in the following reasons. (1) The lack of glacier mass balance modeling in WaterGAP. In Switzerland, summer streamflow over the last decades has increased due to the glacier mass loss (Hänggi & Weingartner, 2012). (2) The impact of electricity prices, which are known to have a significant positive effect on HP (Golombek et al., 2012; Jääskeläinen et al., 2018), is not taken into account in the simulation of reservoir release. (3) The lack of WaterGAP reservoirs (there are no WaterGAP reservoirs in Germany) such that the positive effect of reservoir management on water release during drought cannot be simulated. However, it is still surprising that there was so little HP reduction in Germany according to EIA, as both the observed and the simulated streamflow drought at two streamflow gauging stations on Danube and Rhine, which are downstream of the most important hydropower plants in Germany, are very strong (Figure S5). (4) Simulated reservoir outflow and storage may differ strongly from observations, in particular for smaller reservoirs. For five reservoirs in the US, we compared simulated and observed time series of reservoir storage. The *NSE* for storage of the rather small Big Bend reservoir (494 MW) is negative and the R^2 0.03, while in case of the larger Oahe reservoir (784 MW), a moderate *NSE* of 0.46 and R^2 of 0.68 are achieved (Figure S7).

4.2. Relation Between Streamflow Drought and HP Reduction

Is it possible to estimate HP reduction in whole river basins from streamflow drought as determined from streamflow observations at gauging stations? Total HP in the CRB, for example, is found to be less strongly correlated with streamflow and streamflow deficit at the mouth of the river (cell A in Figure 10) than at the internal cell B (Figure S8). This can be explained by the fact that B is the cell in which the hydropower plant with the largest upstream area is located, while there is no plant at the river stretch between A and B. Correlation between basin-wide HP and streamflow deficits depends largely on distribution of installed capacities of the hydropower plants.

With respect to grid-level streamflow and HP reductions that are exceeded in 1 out of 10 years, computed according to Section 2.6, a weak but significant positive correlation between the two values is observed ($r = 0.43$, $p < 0.001$, Figure 11). The reduction during a deficit period can be larger than 100% of the mean annual value of either streamflow or HP if the deficit event is a multiyear event. For the cells where WaterGAP reservoir plants are located, the Pearson correlation coefficient is even lower ($r = 0.37$, $p < 0.001$). The weak correlations indicate that HP reduction occurring with a probability of 10% in any year is very different from the severity of the streamflow drought. In case of run-of-river plants, a simulated decrease in streamflow only leads to an HP reduction if actual HP is not constrained by installed capacity (Equation 1). Typically, installed capacity puts a cap on HP during the high flow season, leading to differences in the periods of below normal streamflow and below normal HP. In case of various power plants in one grid cell, the higher the hydraulic head of the power plant, the more frequently HP is constrained by installed capacity.

5. Conclusions

In this study, a GHD was compiled. In comparison with EIA country statistics of installed capacity, GHD has proven to be a relatively reliable and complete representation of global hydropower plants. An HP model was developed to simulate, for the period 1975–2016, monthly HP worldwide based on the GHD as well as on outputs of the global hydrological model WaterGAP. Reliability of the monthly streamflow simulated by WaterGAP was tested by comparing simulated values of the streamflow drought indicator SSI3 to observed values at 183 streamflow gauging stations. With a median *NSE* of 0.5, model performance can be regarded as moderate. The country-level HP trends and interannual variabilities are captured quite

well by the HP model, at least for countries with large HP. The ability to simulate HP as well as HP deficits due to drought was tested in the US using statistical data of monthly HP. The HP model can reproduce the observed HP deficit better than the HP itself, and multiyear drought periods in the US and California are clearly identified by the HP model. However, HP reduction during individual drought events can be significantly overestimated or underestimated.

We identified spatially extensive streamflow drought events between 1975 and 2016 worldwide and determined how HP was impacted during these droughts. A global drought risk analysis shows that at the scale of 0.5° grid cell, HP reduction during HP deficit events that occur with a probability of 10% in any year can range between 0% and 267% of mean annual HP, while the respective reductions at the country scale show a narrower range of 3%–79%. Eighteen out of 134 countries suffer from a reduction of more than 40%.

To improve the reliability of the simulated impact of drought on HP, more data on hydropower plants and HP should be made available openly and free of charge. Then, fewer of the hydropower plant attributes in the GHD that are required for simulation of HP would have to be estimated. Equally important, the capability of the WaterGAP model to simulate streamflow and hydraulic head at hydropower plants needs improvement. This requires in particular a better representation of reservoirs and their management, which is a very challenging task.

Data Availability Statement

The global hydropower database (GHD) is freely available for noncommercial use at https://doi.org/10.6084/m9.figshare.11283758. The script of the HP model and the model inputs referred to in this paper, including global drainage direction map DDM30, WaterGAP model output, are also available at this figshare repository. Other data sets for this research can be addressed from World Power Plants Database (WPPD) (Global Energy Observatory, 2019), Global Power Plant Database (GPPD) (World Resources Institute, 2018), Global Reservoir and Dam Database (GRanD) version 2019 (Lehner et al., 2011), HydroSHEDS (Lehner et al., 2006), and International Energy Statistics (EIA, 2019), which have been appropriately cited.

References

Agnew, C. T. (2000). Using the SPI to identify drought. *Drought Network News*, *12*(1), 29–42. Retrieved from http://digitalcommons.unl.edu/droughtnetnews/1

Ali, M. H., Alam, M. R., Haque, M. N., & Alam, M. J. (2012). Comparison of design and analysis of concrete gravity dam. *Natural Resources*, *03*(1), 18–28. https://doi.org/10.4236/nr.2012.31004

Andreadis, K. M., Clark, E. A., Wood, A. W., Hamlet, A. F., & Lettenmaier, D. P. (2005). Twentieth-century drought in the conterminous United States. *Journal of Hydrometeorology*, *6*(6), 985–1001. https://doi.org/10.1175/JHM450.1

Axpo. (2020). *Run-of-river hydropower—In simple terms*. Retrieved from https://www.axpo.com/gb/en/about-us/magazine.detail.html/magazine/renewable-energy/run-of-river-hydropower---in-simple-terms.html

Bakis, R. (2007). The current status and future opportunities of hydroelectricity. *Energy Sources, Part B: Economics, Planning and Policy*, *2*(3), 259–266. https://doi.org/10.1080/15567240500402958

Beames, P., Lehner, B., & Anand, M. (2019). Global Reservoir and Dam (Grand) Database. Technical Documentation, Version 1.3. Retrieved from http://globaldamwatch.org/grand

Benejam, L., Saura-Mas, S., Bardina, M., Solà, C., Munné, A., & García-Berthou, E. (2016). Ecological impacts of small hydropower plants on headwater stream fish: From individual to community effects. *Ecology of Freshwater Fish*, *25*(2), 295–306. https://doi.org/10.1111/eff.12210

Bonsal, B. R., Wheaton, E. E., Chipanshi, A. C., Lin, C., Sauchyn, D. J., & Wen, L. (2011). Drought research in Canada: A review. *Atmosphere-Ocean*, *49*(4), 303–319. https://doi.org/10.1080/07055900.2011.555103

Bunn, S. E., & Arthington, A. H. (2002). Basic principles and ecological consequences of altered flow regimes for aquatic biodiversity. *Environmental Management*, *30*(4), 492–507. https://doi.org/10.1007/s00267-002-2737-0

Cazzaniga, R., Rosa-Clot, M., Rosa-Clot, P., & Tina, G. M. (2019). Integration of PV floating with hydroelectric power plants. *Heliyon*, *5*(6), e1918. https://doi.org/10.1016/j.heliyon.2019.e01918

Charpentier, A. (2011). On the return period of the 2003 heat wave. *Climatic Change*, *109*(3–4), 245–260. https://doi.org/10.1007/s10584-010-9944-0

Department of Energy. (2019). *Types of hydropower plants*. Retrieved from https://www.energy.gov/eere/water/types-hydropower-plants

Döll, P., Fiedler, K., & Zhang, J. (2009). Global-scale analysis of river flow alterations due to water withdrawals and reservoirs. *Hydrology and Earth System Sciences*, *13*(12), 2413–2432. https://doi.org/10.5194/hess-13-2413-2009

Döll, P., & Lehner, B. (2002). Validation of a new global 30-min drainage direction map. *Journal of Hydrology*, *258*(1–4), 214–231. https://doi.org/10.1016/S0022-1694(01)00565-0

Döll, P., Müller Schmied, H., Schuh, C., Portmann, F. T., & Eicker, A. (2014). Global-scale assessment of groundwater depletion and related groundwater abstractions: Combining hydrological modeling with information from well observations and GRACE satellites. *Water Resources Research*, *50*, 5698–5720. https://doi.org/10.1002/2014WR015595

Dracup, J. A., Lee, K. S., & Paulson, E. G. (1980). On the definition of droughts. *Water Resources Research*, *16*(2), 297–302. https://doi.org/10.1029/WR016i002p00297

EIA. (2019). *U.S. Energy Information Administration independent statistics and analysis*. Retrieved from https://www.eia.gov/beta/international/data

Eisner, S. (2016). *Comprehensive evaluation of the WaterGAP3 model across climatic, physiographic, and anthropogenic gradients* (Doctoral dissertation). Kassel, Germany: University of Kassel.

El-Hawary, M. E., & Christensen, G. S. (1979). *Optimal economic operation of electric power systems*. New York: Academic Press.

ENTSO-E. (2017). *Statistical factsheet 2016*. Retrieved from https://docstore.entsoe.eu/Documents/Publications/Statistics/Factsheet/entsoe_sfs_2016_web.pdf

Global Energy Observatory. (2019). *World Power Plants Database*. Retrieved from https://datasource.kapsarc.org/explore/dataset/world-power-plants-list

Golombek, R., Kittelsen, S. A. C., & Haddeland, I. (2012). Climate change: Impacts on electricity markets in Western Europe. *Climatic Change*, *113*(2), 357–370. https://doi.org/10.1007/s10584-011-0348-6

Hambling, D. (2016). *Hydro power falters in persistent drought*. Retrieved from https://www.theguardian.com/news/2016/mar/30/weatherwatch-hambling-venezuela-hydroelectric-dam-guri-dry-reservoirs-colombia?utm_content=buffer2ce55&utm_medium=social&utm_source=twitter.com&utm_campaign=buffer

Hänggi, P., & Weingartner, R. (2012). Variations in discharge volumes for hydropower generation in Switzerland. *Water Resources Management*, *26*(5), 1231–1252. https://doi.org/10.1007/s11269-011-9956-1

Haslinger, K., & Blöschl, G. (2017). Space–time patterns of meteorological drought events in the European Greater Alpine region over the past 210 years. *Water Resources Research*, *53*, 9807–9823. https://doi.org/10.1002/2017WR020797

Herrera-Estrada, J. E., Diffenbaugh, N. S., Wagner, F., Craft, A., & Sheffield, J. (2018). Response of electricity sector air pollution emissions to drought conditions in the western United States. *Environmental Research Letters*, *13*(12), 124032. https://doi.org/10.1088/1748-9326/aaf07b

House, C., Way, S. N., & Sutton, L. (2018). *The world's water battery: Pumped hydropower storage and the clean energy transition*. United Kingdom.

IEA. (2019). *International Energy Agency: Hydropower tracking clean energy progress*. Retrieved from https://www.iea.org/tcep/power/renewables/hydropower

IHA. (2018). *International Hydropower Association: 2018 hydropower status report*. London, United Kingdom.

Jääskeläinen, J., Veijalainen, N., Syri, S., Marttunen, M., & Zakeri, B. (2018). Energy security impacts of a severe drought on the future Finnish energy system. *Journal of Environmental Management*, *217*, 542–554. https://doi.org/10.1016/j.jenvman.2018.03.017

Kling, H., Fuchs, M., & Paulin, M. (2012). Runoff conditions in the upper Danube basin under an ensemble of climate change scenarios. *Journal of Hydrology*, *424–425*, 264–277. https://doi.org/10.1016/j.jhydrol.2012.01.011

Krysanova, V., Zaherpour, J., Didovets, I., Gosling, S. N., Gerten, D., Hanasaki, N., et al. (2020). How evaluation of global hydrological models can help to improve credibility of river discharge projections under climate change. *Climatic Change*, *163*, 1353–1377. https://doi.org/10.1007/s10584-020-02840-0

Laaha, G., Gauster, T., Tallaksen, L. M., Vidal, J.-P., Stahl, K., Prudhomme, C., et al. (2017). The European 2015 drought from a hydrological perspective. *Hydrology and Earth System Sciences*, *21*, 3001–3024. https://doi.org/10.5194/hess-21-3001-2017

Lehner, B., Liermann, C. R., Revenga, C., Vörösmarty, C., Fekete, B., Crouzet, P., et al. (2011). High-resolution mapping of the world's reservoirs and dams for sustainable river-flow management. *Frontiers in Ecology and the Environment*, *9*(9), 494–502. https://doi.org/10.1890/100125

Lehner, B., Verdin, K., & Jarvis, A. (2006). *HydroSHEDS technical documentation*. Washington, DC: World Wildlife Fund US. Retrieved from http://hydrosheds.cr.usgs.gov

Liu, Y., Zhu, Y., Ren, L., Singh, V. P., Yong, B., Jiang, S., et al. (2019). Understanding the spatiotemporal links between meteorological and hydrological droughts from a three-dimensional perspective. *Journal of Geophysical Research: Atmospheres*, *124*, 3090–3109. https://doi.org/10.1029/2018JD028947

Masih, I., Maskey, S., Mussá, F. E. F., & Trambauer, P. (2014). A review of droughts on the African continent: A geospatial and long-term perspective. *Hydrology and Earth System Sciences*, *18*(9), 3635–3649. https://doi.org/10.5194/hess-18-3635-2014

Mukheibir, P. (2013). Potential consequences of projected climate change impacts on hydroelectricity generation. *Climatic Change*, *121*(1), 67–78. https://doi.org/10.1007/s10584-013-0890-5

Müller Schmied, H., Cáceres, D., Eisner, S., Flörke, M., Herbert, C., Niemann, C., et al. (2021). The global water resources and use model WaterGAP v2.2d: Model description and evaluation. *Geoscientific Model Development*, *14*(2), 1037–1079. https://doi.org/10.5194/gmd-14-1037-2021

Müller Schmied, H., Eisner, S., Franz, D., Wattenbach, M., Portmann, F. T., Flörke, M., & Döll, P. (2014). Sensitivity of simulated global-al-scale freshwater fluxes and storages to input data, hydrological model structure, human water use and calibration. *Hydrology and Earth System Sciences*, *11*(2), 1583–1649. https://doi.org/10.5194/hess-18-3511-2014

Nash, J. E., & Sutcliffe, J. V. (1970). River flow forecasting through conceptual models part I—A discussion of principles. *Journal of Hydrology*, *10*(3), 282–290. https://doi.org/10.1016/0022-1694(70)90255-6

Schewe, J., Gosling, S. N., Reyer, C., Zhao, F., Ciais, P., Elliott, J., et al. (2019). State-of-the-art global models underestimate impacts from climate extremes. *Nature Communications*, *10*(1), 1005. https://doi.org/10.1038/s41467-019-08745-6

Schill, W., & Kemfert, C. (2011). Modeling strategic electricity storage: The case of pumped hydro storage in Germany. *Energy Journal*, *32*(3), 59–87. https://doi.org/10.5547/ISSN0195-6574-EJ-Vol32-No3-3

Singh, S. C., & Sally, M. (2020). *Electricity supply to face disruptions amid high demand and acute water shortage*. Retrieved from https://economictimes.indiatimes.com/industry/energy/power/electricity-supply-to-face-disruptions-amid-high-demand-and-acute-water-shortage/articleshow/51675775.cms

Smith, R. L. (1984). *Threshold methods for sample extremes* (Vol. 131, pp. 621–638). Dordrecht, The Netherlands: Springer. https://doi.org/10.1007/978-94-017-3069-3_48

Spinoni, J., Naumann, G., Vogt, J. V., & Barbosa, P. (2015). The biggest drought events in Europe from 1950 to 2012. *Journal of Hydrology: Regional Studies*, *3*, 509–524. https://doi.org/10.1016/j.ejrh.2015.01.001

Stanton, M. C. B., Dessai, S., & Paavola, J. (2016). A systematic review of the impacts of climate variability and change on electricity systems in Europe. *Energy*, *109*, 1148–1159. https://doi.org/10.1016/j.energy.2016.05.015

UDI. (2013). *World Electric Power Plants Database*. Retrieved from https://www.spglobal.com/platts/ko/products-services/electric-power/world-electric-power-plants-database

UNCTAD. (2017). *The least developed countries report 2017*. New York/Geneva, Switzerland: United Nations Conference on Trade and Development.

Van Vliet, M. T. H., Sheffield, J., Wiberg, D., & Wood, E. F. (2016). Impacts of recent drought and warm years on water resources and electricity supply worldwide. *Environmental Research Letters*, *11*(12), 124021. https://doi.org/10.1088/1748-9326/11/12/124021

Van Vliet, M. T. H., van Beek, L. P. H., Eisner, S., Flörke, M., Wada, Y., & Bierkens, M. F. P. (2016). Multi-model assessment of global hydropower and cooling water discharge potential under climate change. *Global Environmental Change*, *40*, 156–170. https://doi.org/10.1016/j.gloenvcha.2016.07.007

Van Vliet, M. T. H., Wiberg, D., Leduc, S., & Riahi, K. (2016). Power-generation system vulnerability and adaptation to changes in climate and water resources. *Nature Climate Change*, *6*(4), 375–380. https://doi.org/10.1038/nclimate2903

Vicente-Serrano, S. M., López-Moreno, J. I., Beguería, S., Lorenzo-Lacruz, J., Azorin-Molina, C., & Morán-Tejeda, E. (2011). Accurate computation of a streamflow drought index. *Journal of Hydrologic Engineering*, *17*(2), 318–332. https://doi.org/10.1061/(ASCE)HE.1943-5584.0000433

Wan, W., Wang, H., & Zhao, J. (2020). Hydraulic potential energy model for hydropower operation in mixed reservoir systems. *Water Resources Research*, *56*, e2019WR026062. https://doi.org/10.1029/2019WR026062

Weedon, G. P., Balsamo, G., Bellouin, N., Gomes, S., Best, M. J., & Viterbo, P. (2014). The WFDEI meteorological forcing data set: WATCH Forcing Data methodology applied to ERA-Interim reanalysis data. *Water Resources Research*, *50*, 7505–7514. https://doi.org/10.1002/2014WR015638

World Resources Institute. (2018). *Global Power Plant Database*. Published on Resource Watch and Google Earth Engine. Retrieved from http://datasets.wri.org/dataset/globalpowerplantdatabase

Yildiz, V., & Vrugt, J. A. (2019). A toolbox for the optimal design of run-of-river hydropower plants. *Environmental Modelling & Software*, *111*, 134–152. https://doi.org/10.1016/j.envsoft.2018.08.018

Zaherpour, J., Gosling, S. N., Mount, N., Schmied, H. M., Veldkamp, T. I. E., Dankers, R., et al. (2018). Worldwide evaluation of mean and extreme runoff from six global-scale hydrological models that account for human impacts. *Environmental Research Letters*, *13*, 065015. https://doi.org/10.1088/1748-9326/aac547

Zhang, L., & Zhou, T. (2015). Drought over East Asia: A review. *Journal of Climate*, *28*(8), 3375–3399. https://doi.org/10.1175/JCLI-D-14-00259.1

Zhao, T., Zhao, J., & Yang, D. (2014). Improved dynamic programming for hydropower reservoir operation. *Journal of Water Resources Planning and Management*, *140*, 365–374. https://doi.org/10.1061/(ASCE)WR.1943-5452.0000343

Zhou, Z., Shen, Z., Shi, X., & Li, T. (1997). *Water resources and hydropower planning*. Beijing, China: China Water and Power Press.

References From the Supporting Information

Clarke, K. A. (2007). A simple distribution-free test for nonnested model selection. *Political Analysis*, *15*(3), 347–363. https://doi.org/10.1093/pan/mpm004

Gudmundsson, L. S., & Stagge, J. H. (2016). *SCI: Standardized Climate Indices such as SPI, SRI or SPEIR 32 package version 1.0*. Retrieved from https://cran.r-project.org/web/packages/SCI/SCI.pdf

Krause, P., Boyle, D. P., & Bäse, F. (2005). Comparison of different efficiency criteria for hydrological model assessment. *Advances in Geosciences*, *5*, 89–97. https://doi.org/10.5194/adgeo-5-89-2005

McKee, T. B., Doesken, N. J., & Kleist, J. (1993). *The relationship of drought frequency and duration to time scales*. Paper presented at American Meteorological Society 8h Conference on Applied Climatology, Anaheim, California.

Rigby, R. A., & Stasinopoulos, D. M. (2005). Generalized additive models for location, scale and shape (with discussion). *Journal of the Royal Statistical Society: Series C (Applied Statistics)*, *54*(3), 507–554. https://doi.org/10.1111/j.1467-9876.2005.00510.x